Chapter 3
Ice and Its Formation

Amir Haji-Akbari

3.1 Introduction

Freezing of water into ice is a ubiquitous phenomenon that has fascinated mankind for millennia. In addition to biological cells (Padayachee et al. 2009), ice formation can occur in a wide variety of other environments, including atmospheric clouds (Baker 1997; Carslaw et al. 2002), soil (Chamberlain and Gow 1979), freshwater resources (Beltaos and Prowse 2009), aircraft (Potapczuk 2013), and aviation and transportation infrastructure (Ye et al. 2013). The ubiquity and relative ease of freezing water have, since antiquity, been used in applications such as traditional medicine (Yang and Mochizuki 2003), transportation (Li et al. 2013a), mummification (Cockburn et al. 1998), and food preservation (Varshney and Singh 2015) and processing (Arbuckle 1986). Ice formation also plays a pivotal role in many natural processes, such as cloud microphysics (Fowler et al. 1996; Herbert et al. 2015). For instance, freezing of supercooled microdroplets of water in atmospheric clouds triggers a cascade of events that eventually result in precipitation. Predicting the spatiotemporal distribution of ice droplets within a cloud is, therefore, an important—and yet challenging—component of climate modeling (Wilson and Ballard 1999).

Freezing is usually disruptive in biological systems, and can result in cell death. Not only can ice particles damage cell membranes (Muldrew and McGann 1990, 1994), but they can also result in cold denaturation of proteins (Privalov 1990). A large portion of this book is dedicated to understanding how antifreeze proteins (AFPs) prevent and/or control ice formation within cells and organisms. In order to understand how AFPs function, however, it is first necessary to have a fundamental

A. Haji-Akbari (✉)
Department of Chemical & Environmental Engineering, Yale University, New Haven, CT, USA
e-mail: amir.hajiakbaribalou@yale.edu

H. Ramløv, D. S. Friis (eds.), *Antifreeze Proteins Volume 1*,
https://doi.org/10.1007/978-3-030-41929-5_3

understanding of the microscopic structure of ice, and the thermodynamics and kinetics of its formation.

Considering the ubiquity of freezing and its important ramifications in many disciplines, the question of ice formation has been extensively studied, and this current chapter offers only a brief introduction. In this context, the term "ice" refers to any condensed phase of water that exhibits mechanical properties of a solid. This notion encompasses both *crystalline ices*, i.e., structures in which the oxygen atoms of constituent water molecules are arranged into periodic lattices, and *amorphous ices*, or kinetically arrested glassy states of liquid water. Like almost everything else about water, crystalline and glassy ices exhibit various interesting anomalies some of which will be discussed in this chapter.

This chapter is organized as follows. Section 3.2 is dedicated to a brief discussion of the thermodynamics of crystallization. Section 3.3 discusses ice anomalies, including water's complicated phase diagram and its ability to form open-network crystals. Section 3.4 is dedicated to ice I, the thermodynamically stable crystalline phase of water under ambient conditions, and discusses the thermodynamics and kinetics of its formation in pure water and aqueous solutions. The chapter is concluded with a discussion of amorphous ices in Sect. 3.5.

3.2 Physics of Crystallization

Before discussing ice, its anomalies, and the thermodynamics and kinetics of its formation, it is useful to provide a quick precept of some basic thermodynamic concepts that will be frequently referred to in this chapter. According to classical thermodynamics, a system will reach thermodynamic equilibrium by minimizing its *free energy*. The precise notion of what constitutes free energy, i.e., the particular thermodynamic function that needs to be minimized at equilibrium, depends on the thermodynamic *ensemble* or the set of thermodynamic variables controlled during an experiment. In most experiments, it is the temperature and pressure that are kept constant, and therefore the quantity that needs to minimize at equilibrium is the *Gibbs free energy*, G, which is related to internal energy E, volume V, and entropy S by:

$$G = E + PV - TS \tag{3.1}$$

Here, P and T are pressure and temperature, respectively. Therefore, under isothermal isobaric conditions, a crystal becomes more stable when its molar Gibbs free energy—also known as *chemical potential*, μ—is smaller than that of its competitors.

Crystallization is a *first-order phase transition* in the sense that it involves discontinuities in first derivatives of Gibbs free energy, such as enthalpy, H, and volume. For instance, a latent heat of fusion is released during crystallization, which is due to the fact that the solid has a lower enthalpy than the liquid. Similarly, the

crystal and the liquid of the same substance usually have different densities. Despite this discontinuity in first derivatives, a crystal and a liquid can coexist under conditions at which their chemical potentials are equal. The loci of temperatures and pressures at which this can happen are called the *coexistence line*, with its slope given by the *Clausius–Clapeyron* equation:

$$\frac{dP}{dT} = \frac{\Delta h_{\mathrm{m}}}{T \Delta v_{\mathrm{m}}} \tag{3.2}$$

Here, Δh_{m} is the latent enthalpy of fusion and Δv_{m} is the difference between specific volumes of liquid and the solid. Each point on a solid–liquid coexistence line is technically a *melting point*, but the term usually refers to the coexistence temperature at ambient pressure, i.e., at 1 bar. The temperature and pressure at which a solid–liquid coexistence line intersects the solid–gas and liquid–gas coexistence lines are called a *triple point*. Also, coexistence lines that separate two disordered phases, such as gas and liquid, usually end in a *critical point* at which the transition between the two phases becomes *second order* and the macroscopic distinction between them, e.g., in terms of density and enthalpy difference, disappears. Beyond the critical point, a transformation between the two phases will become continuous, i.e., without any discontinuities in thermodynamic functions.

3.3 Anomalies of Crystalline Ices

Water is a material with numerous anomalous properties, the origins of which are far from fully understood (Debenedetti 2003; Gallo et al. 2016). In order to understand anomalies associated with crystalline ices, it is first necessary to discuss what we expect from the crystallization of a typical single-component liquid. For most materials, liquid–solid transition will result in the formation of a *single* thermodynamically stable crystalline solid, which will always be *denser* than the liquid at coexistence. Therefore, according to Eq. (3.2), the coexistence line will have a positive slope. From a molecular perspective, this behavior emanates from the fact that intermolecular interactions between most small molecules are nonspecific and nondirectional in nature. Therefore, only the densely packed crystalline structures can be energetically favored, and since there are not very many such structures (Hales 2006; Damasceno et al. 2012), the phase diagram will be simple, with one—or a handful of—crystalline phases only.

Water is a material that deviates from this generic picture as it not only can exist in several distinct crystalline forms, but it can also form crystals that are less dense than the liquid. These two anomalies will be discussed at length in Sects. 3.3.1 and 3.3.2, respectively. A simple conceptual framework to understand them, however, is to note the importance of hydrogen bonding in water. As strong and highly directional specific interactions, hydrogen bonds contribute so strongly to the internal energy of condensed phases of water that such phases can only be stable if their

constituent molecules form as many hydrogen bonds with their neighbors as possible. As will be discussed later, this constraint can be satisfied by a wide variety of permitted—including some open network—crystalline structures. This is unlike simple liquids, which, as discussed above, mostly form densely packed crystals.

3.3.1 Polymorphism in Water

In materials science, *polymorphism* refers to a material's ability to form distinct crystalline structures, i.e., structures with distinct sets of point symmetry operations. Each such structure is typically called a *polymorph*. As explained above, most single-component systems only form one thermodynamically stable polymorph, and therefore have simple phase diagrams with one solid/liquid/gas triple point and one liquid/gas critical point. Water is a notable exception, as evidenced by its very complex phase diagram (Fig. 3.1), and has 18 experimentally observed crystalline polymorphs, denoted by Roman numerals according to their chronological order of discovery. Some of these polymorphs, including five thermodynamically

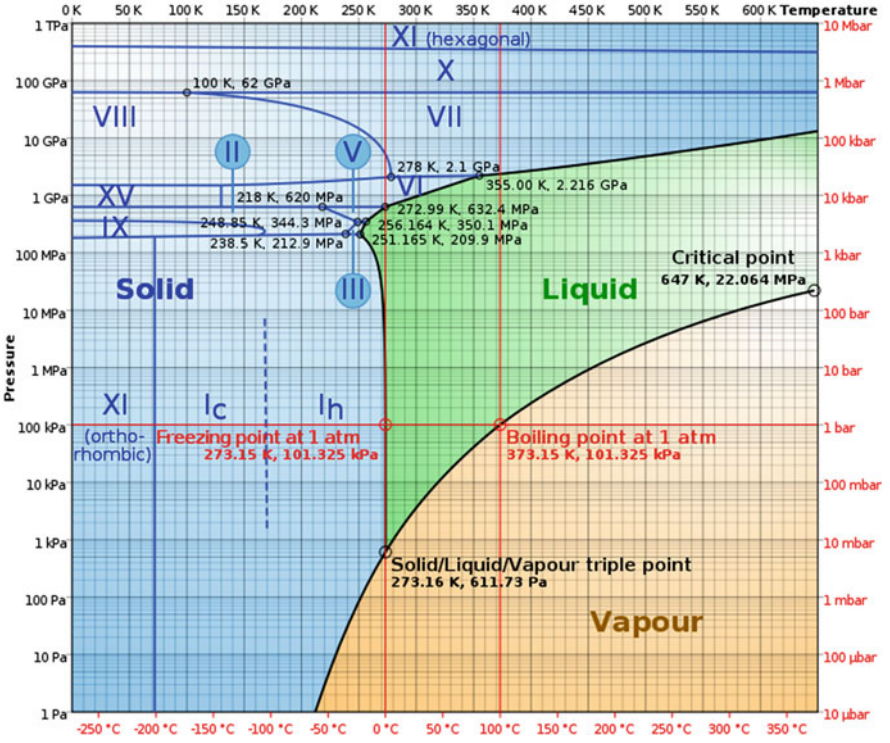

Fig. 3.1 Equilibrium phase diagram of water. Note that ice can exist in many different polymorphs. Reproduced from Zhang et al. (2015)

stable ones, can directly form within—and coexist with—liquid water, while the remaining ones are only accessible through solid–solid transformations. Due to this rich polymorphism, the phase diagram of water has five solid–solid–liquid (Bridgman 1912; Schwager et al. 2004; Goncharov et al. 2005, 2009), eight solid–solid–solid (Bridgman 1912; Kauzmann and Eisenberg 1969; Fletcher 1970; Mercury et al. 2001; Song et al. 2003; Salzmann et al. 2009; Yen and Chi 2015), and one gas–solid–solid (Petrenko and Whitworth 1999) triple points, in addition to the generic gas–liquid–solid triple point commonly observed for other materials. Despite their structural differences, all these crystalline ices are similar in the sense that every water molecule in them forms exactly four hydrogen bonds with its neighbors, two as a proton donor and two as a proton acceptor (Zheligovskaya and Malenkov 2006). These constraints are typically referred to as *Bernal Fowler rules* or *ice rules* (Bernal and Fowler 1933).

Ice I is the most common polymorph of ice, and forms at ambient pressures. It has two polymorphs that are stacking variants of one another: the thermodynamically stable *hexagonal ice* (I_h) and the thermodynamically metastable *cubic ice* (I_c). The structure of ice I and the thermodynamics and kinetics of its formation will be discussed in detail in Sect. 3.4. Other ice polymorphs can only form under non-ambient conditions, such as very high pressures, and/or very low temperatures. Historically, the first non-ambient polymorph of ice is ice II, which was discovered in the beginning of the twentieth century, and has a rhombohedral unit cell composed of 12 water molecules (Kamb 1964). Ice II can be obtained from ice I at 198 K and 300 MPa (Fuentes-Landete et al. 2015). Since then, 16 more ice polymorphs have been discovered. The most recent polymorphs, ice XVII and XVIII, were only discovered in 2016 (del Rosso et al. 2016a, b) and 2019 (Millot et al. 2019), respectively. Ice polymorphs span a wide range of densities (from 0.85 g cm^{-3} in the case of ice XVII (del Rosso et al. 2016a, b) to 2.785 g cm^{-3} in the case of ice X (Hemley et al. 1987) and ~3 g cm^{-3} in the case of ice XVIII (Millot et al. 2019)) and have unit cells with as few as two molecules—e.g., in the case of ice VII (Kamb and Davis 1964) and ice X (Hemley et al. 1987)—to 136 molecules—e.g., in the case of ice XVI (Falenty et al. 2014).

Polymorphism in water is very rich and unprecedented even in comparison to other tetrahedral liquids such as silicon (Jones and Stevanovíc 2017), which also have multiple polymorphs. One important factor that contributes to this richness is the asymmetric nature of a hydrogen bond. In other words, a hydrogen atom that bridges two oxygen atoms is covalently bonded—and is, therefore, closer—to one of those oxygens. This asymmetry allows for degeneracy in assigning protons to oxygen that are located on a periodic lattice, with the number of all possible assignments scaling exponentially with the number of water molecules in the lattice.[1] There are usually small energetic differences between these distinct arrangements, but such differences are usually too small for any particular arrangement to be

[1]Note that a vanishingly small fraction of such arrangements will have nonzero electrostatic dipole or quadrupole moments. Such structures will have a vanishingly small probability of emerging in a proton-disordered phase.

favored unless at very low temperatures. Therefore, ice polymorphs at higher temperatures are usually *proton-disordered*, and the entropy associated with such proton disorder lowers their free energy and enhances their thermodynamic stability. When temperatures are sufficiently low, however, the entropic gain associated with proton disorder will become smaller, and eventually a transition into a proton-ordered phase will take place. Without such proton disorder–order transitions, far fewer ice polymorphs would have existed, as twelve of the eighteen known polymorphs come in pairs that only differ in their proton order (Fuentes-Landete et al. 2015). For instance, ice I transforms into its proton-ordered counterpart, ice XI, at 72 K (Fukazawa et al. 1998). Ice X is the only polymorph in which this hydrogen bonding asymmetry is broken, and each proton is equally spaced between the two oxygens that it bridges (Hirsch and Holzapfel 1984).

In addition to these experimentally observed polymorphs, there are many more polymorphs whose existence has been predicted using computational methods such as density functional theory (Gross and Dreizler 2013) or classical force fields (Guillot 2002; Vega and Abascal 2011). Such polymorphs are typically known as *computer ices*, and are usually difficult to isolate in experiments. One important class of computer ices constitutes those that are predicted to form at experimentally inaccessible pressures. The most notable example is *metallic ice*, which is predicted to form at pressures above 4.8 TPa. Metallic ice has the crystallographic space group C_2/m, and its electrons are delocalized like a metal (Hermann et al. 2012). [A possible experimental candidate for metallic ice has only been observed recently, though its electronic properties vis-a-vis the diffusion of protons are yet to be confirmed (Millot et al. 2019).]

Not all computer ices are expected to form at high pressures. For instance, ice 0, which was recently proposed as a precursor for the formation of ice I, has an open tetragonal structure with a unit cell composed of 12 water molecules (Russo et al. 2014). In principle, any crystalline structure that is tetrahedral, satisfies ice rules, and is mechanically stable, can at least be thermodynamically metastable. As to which of these computer ices can form in reality is an open question that can only be addressed experimentally.

The polymorphs discussed so far can form—or be stable—in the bulk. In ultra-confined geometries, such as nanotubes and nanopores, however, water's hydrogen bond network can be disrupted, which can, in turn, culminate in the formation of novel ice polymorphs. Such polymorphs are typically called *two-dimensional ices* and can only exist under the geometrical constraints induced as a result of confinement. Historically, such two-dimensional ices were originally discovered in molecular simulations, but the existence of some of them has been recently confirmed in experiments (Zhao et al. 2014b). 2D ices can exist in many different forms, including monolayers (Zangi and Mark 2003; Kumar et al. 2005; Bai et al. 2010; Kaneko et al. 2013; Zhao et al. 2014a; Chen et al. 2016; Corsetti et al. 2016; Barati Farimani and Aluru 2016), bilayers (Koga et al. 1997; Kastelowitz et al. 2010; Johnston et al. 2010; Algara-Siller et al. 2015; Zhu et al. 2016; Chen et al. 2017), and ice nanotubes (Koga et al. 2001; Bai et al. 2006; Takaiwa et al. 2008). Unconventional 2D ice polymorphs can, in theory, form in biological systems due to the presence of ultra-

confined geometries within biological cells. Such possibilities have, however, not been thoroughly investigated.

3.3.2 Formation of Open-Network Crystals

Another interesting consequence of hydrogen bonding in water is its ability to form open-network crystalline structures, or phases that are less dense than the liquid. This rather striking feature is only shared by a handful of other small molecules, e.g., Group IV elements such as carbon and germanium (Brygoo et al. 2007; Jayaraman et al. 1963). Open-network ices typically reside in the low-P region of the phase diagram. Among thermodynamically stable ices, only ice I has an open structure and is ≈8% less dense than liquid water at coexistence. The remaining four ice polymorphs that can coexist with liquid water, i.e., ices III, V, VI, and VII, are all denser than the liquid.

The fact that ice I is less dense than liquid water has important physiological consequences. First of all, one of the reasons that makes ice formation so disruptive to biological cells is the volumetric expansion of liquid water upon freezing. Therefore, ice particles that form intracellularly or extracellularly will occupy a larger volume than the liquid and can, therefore, exert mechanical stress on cell membranes (Meryman 1956). Ecologically, however, this density anomaly is critical to the sustenance of life in lakes and rivers during cold winters, since such freshwater resources freeze from the top and the marine life can still survive within the liquid entrapped below the ice cap.

Another important consequence of this density anomaly is what is known as *pressure melting*. Indeed, for a liquid that is denser than its crystal, such as liquid water and ice I, $\Delta v_m < 0$ and according to Eq. (3.2), the solid–liquid coexistence line will have a negative slope. This will imply that ice I can become unstable upon both heating and pressurization. At temperatures above 251 K, ice will eventually melt at some pressure below ~210 MPa (Fuentes-Landete et al. 2015). Pressure–melting of ice is believed to play a pivotal role in glacier mobility (Weertman 1957).

Ice I is not the only open-network crystal of pure water. In recent years, several other such polymorphs have been discovered. These ices are metastable, can usually form at negative pressures only, and are obtained by exposing two-component crystals of water and small gaseous molecules to vacuum. For instance, ice XVI is obtained by vacuum pumping a clathrate hydrate of neon (Falenty et al. 2014). Gas hydrates are crystalline solids in which water molecules form cages that encompass small guest molecules such as methane, carbon dioxide, hydrogen, and neon (Maslin et al. 2010; Knott et al. 2012), and will be discussed in further detail in Chap. 12 of Vol. 2. At ambient pressures, such cages will collapse in the absence of guest molecules. Applying negative pressure to such hydrates, however, can generate a driving force for the removal of the guest molecules and the subsequent formation of *guest free clathrates*. Ice XVI is the first experimentally observed guest-free clathrate of water, even though guest-free clathrates had been previously observed in other

systems such as germanium (Guloy et al. 2006). Not all open-network ice polymorphs are obtained from applying negative pressures to clathrate hydrates. For instance, ice XVII (del Rosso et al. 2016a, b) is the guest-free variant of a two-component crystal composed of water and hydrogen, which has a quartz-like structure (Strobel et al. 2016).

3.4 Ice I: The Ambient and Biologically Relevant Form of Ice

As mentioned above, ice I is the only ice polymorph that forms at ambient pressures, and is, therefore, the only form of crystalline ice relevant to biological systems. This section is dedicated to a discussion of its structure and the thermodynamics and kinetics of its formation in pure water and aqueous solutions.

3.4.1 Structure of Ice I

As mentioned in Sect. 3.3.1, every water molecule in a crystalline ice forms hydrogen bonds with four of its neighbors in accordance with Bernard–Fowler rules. In ice I, each molecule has exactly four neighbors in its first hydration shell, and forms hydrogen bonds with all of them. These nearest neighbors are all arranged tetrahedrally around the central molecule with an average O–O distance of 0.276 nm. As will be discussed in Sect. 3.5, this local tetrahedral arrangement is not unique to ice I and can exist in amorphous ices as well. What distinguishes ice I, however, is a hierarchy of structures that culminate in a periodic lattice with long-range translational order. There are different ways of describing this hierarchy, two of which will be discussed here.

The first approach is based on viewing ice I as a layered structure with water molecules within each layer organizing into hexagons. The two-dimensional projection of each such layer will thus be the *honeycomb* lattice (Fig. 3.2a, e). Due to the tetrahedral nature of hydrogen bonding, however, these layers are not flat, and their constituent hexagons adopt chair-like configurations. In Fig. 3.2b, f, the oxygens that are above and below the average plane of a hexagon are depicted in purple and green, respectively. Among the four hydrogen bonds that each molecule forms, three are with molecules that are within the same layer, while the fourth is with a molecule in an adjacent layer. This constraint is, however, not sufficient for uniquely determining the arrangement of adjacent layers, and ice I can, therefore, exist in different stacking variants, also known as *polytopes*.

The most commonly known ice I polytope is *hexagonal ice*, which is denoted by I_h and has the space group $P6_3/mmc$ (Fig. 3.2a–d). In hexagonal ice, adjacent layers are mirror images of one another, and each upward oxygen (purple) is adjacent to a

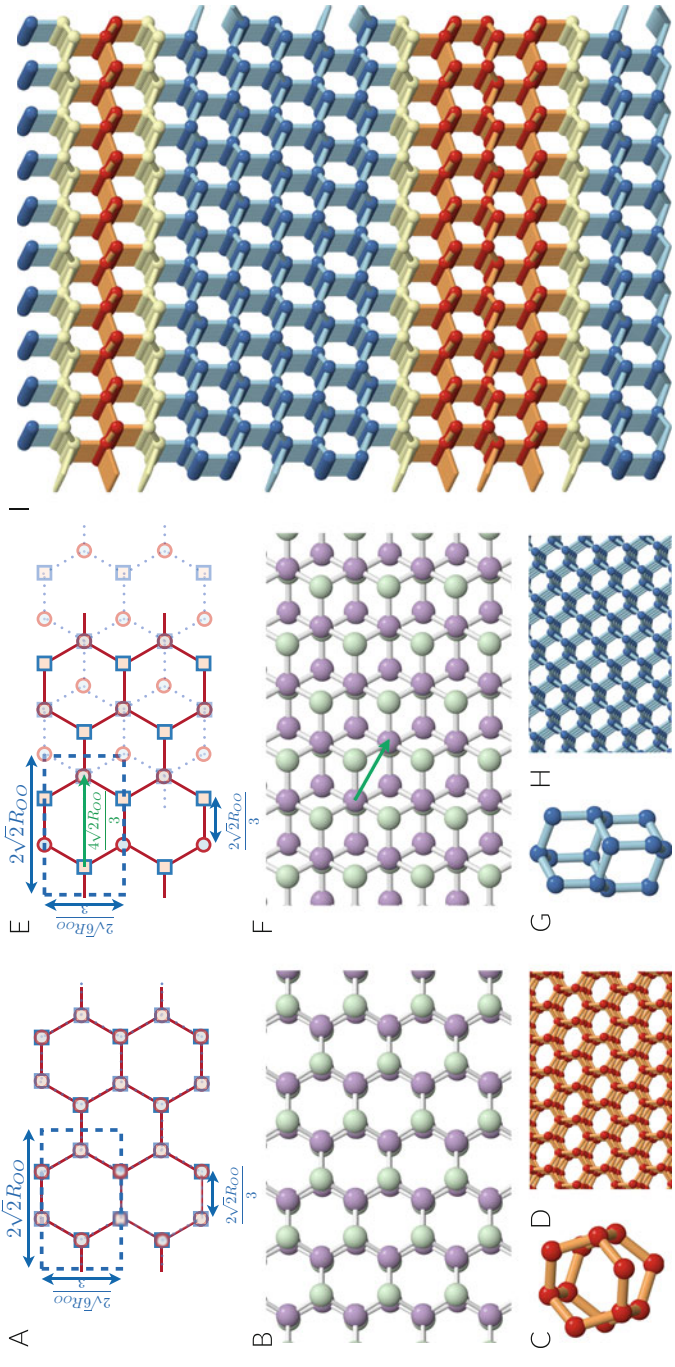

Fig. 3.2 Polymorphs of ice I. **(a–d)** Hexagonal ice, I_h, in which adjacent layers are reflected with respect to one another, with their up (square) and down (circular) oxygens sitting on top of one another **(a, b)**. This culminates in a layered structure **(d)** composed of hexagonal cages **(c)**. **(e–h)** Cubic ice, I_c, in which adjacent layers have the same orientation, but are shifted with respect to one another by $4\sqrt{2}R_{OO}/3$. **(e, f)** The corresponding layered structure **(h)** is composed of double-diamond cages **(g)**. **(i)** Stacking disordered ice, with hexagonal and cubic layers depicted in red and blue, respectively. Stacking faults are shown in light yellow

downward oxygen (green) in the layer above it (Fig. 3.2b). Ice I_h, therefore, has a stacking sequence of *ABAB* $\cdots$, with *A* and *B* corresponding to layers related to one another via reflection. The second idealized polytope of ice I is cubic ice (Fig. 3.2e–h), which is denoted by I_c and has the space group $Fd3m$ (König 1943). In I_c, adjacent layers are not mirror images of one another but are instead related to one another via a translation by a distance $4\sqrt{2}r_{OO}/3$. Since each layer will be recovered after three such translations, I_c has a stacking sequence of *ABCABC* $\cdots$. Both cubic and hexagonal ices are proton disordered, with a zero-point entropy of 3.41 J mol^{-1} K^{-1} (Kolafa 2014).

These two polytopes can also be understood in terms of their constituent topological building blocks (Haji-Akbari and Debenedetti 2015), as hexagonal and cubic ices are composed of hexagonal and double-diamond cages, respectively. Hexagonal cages (HCs) (Fig. 3.2c) are anisotropic motifs composed of five hexagons. Two of these hexagons participate in stacking layers, have chair like conformations, and are known as *basal* faces, while the remaining three have boat-like conformations and are referred to as *prismatic* faces. Double-diamond cages (DDCs) (Fig. 3.2g) are, however, structurally compact and are composed of six identical chair-like hexagons surrounding an internal chair-like hexagon that participates in the stacking layer. A DDC can, therefore, be viewed as two tetrahedra sitting on top of one another, and rotated with respect to each other by 60°.

Since these two polytopes differ in their stacking sequence only, their lattice energies are almost identical. Hexagonal ice is, however, thermodynamically more stable (Handa et al. 1986), a fact that has recently been attributed to its lower anharmonic nuclear vibrational energy (Engel et al. 2015). Cubic ice, which is thermodynamically metastable, has never been isolated in its single crystalline form. It is instead an idealized representation of ices that form at very low temperatures (Dowell and Rinfret 1960; Kohl et al. 2000; Murray et al. 2005; Shilling et al. 2006) and/or in ultra-confined geometries such as nano-droplets (Johari 2005) and nano-pores (Steytler et al. 1983; Morishige and Uematsu 2005; Morishige et al. 2009). Such metastable ices are usually a mixture of cubic and hexagonal stacks with a high (≈60–70%) fraction of cubic stacks, and are collectively referred to as *stacking disordered ice* I_{sd} (Fig. 3.2i). Geometrically, I_{sd} can be constructed in a layer-by-layer fashion by randomly applying reflection or translation to any new layer that is added on top of the existing layers. The importance of cubic ice and stacking disorder in ice nucleation will be discussed in detail in Sect. 3.4.2. The kinetics of transformation from I_{sd} into the thermodynamically stable I_h is, however, very slow at low temperatures (Murray et al. 2005; Gainaru et al. 2018). Further information about stacking disordered ice can be found in a review by Malkin et al. (2015).

3.4.1.1 Crystallography of Hexagonal Ice

Considering the importance of I_h in biological systems, it is worthwhile to discuss its crystallography in further detail. I_h belongs to the hexagonal family of crystals, and has two crystallographic axes (Fig. 3.3a). Its first major axis is denoted by c and is perpendicular to the basal faces of HCs. Its second major axis—denoted by a—lies on a plane perpendicular to c and points toward the vertices of individual hexagons. Note that there are three equivalent directions for a, denoted by $\mathbf{a}_1$, $\mathbf{a}_2$, and $\mathbf{a}_3$ in Fig. 3.3a. These three degenerate vectors, along with $\mathbf{c}$, uniquely determine the unit cell of hexagonal ice. Using such a mathematically overdetermined basis set might seem strange at first, but has important mathematical advantages explained in Allen (2010).

In principle, it is possible to define countably infinite number of distinct crystallographic planes of any crystal by constructing integer valued linear combinations of its basis set. Most such planes will be experimentally uninteresting, either due to their high surface energy, or because of their similarity to simpler crystallographic planes with smaller integer indices. Hexagonal ice has three major crystallographic planes. The *basal plane* (or the 0001 plane) is perpendicular to the c-axis and correspond to basal faces of HCs (Fig. 3.3b). The basal plane is the lowest energy plane of I_h and has a surface enthalpy of 5.57 μJ cm^{-2} (Shultz et al. 2015). The *primary prismatic plane*—or the $01\bar{1}0$ plane—is perpendicular to the a-axis (Fig. 3.3c), and has a surface enthalpy of 5.95 μJ cm^{-2} (Shultz et al. 2015), while

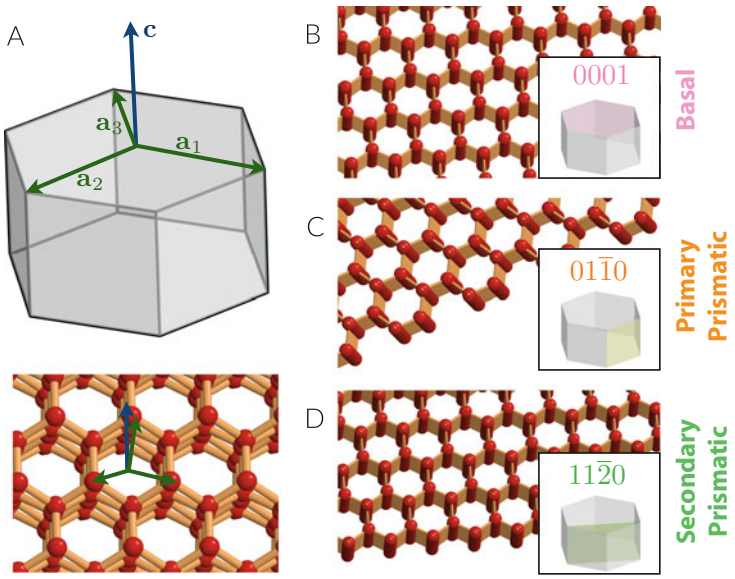

Fig. 3.3 Major crystallographic planes of hexagonal ice. (**a**) Major crystallographic axes overlaid on the structure of I_h. Note that there are three equivalent a axes. (**b**) Basal, (**c**) primary prismatic and (**d**) secondary prismatic planes

the *secondary prismatic plane*—or the $11\bar{2}0$ plane—is perpendicular to a prismatic face and has a surface enthalpy of 6.90 μJ cm^{-2} (Shultz et al. 2015). These crystallographic planes are important in understanding the function of antifreeze proteins, as different AFPs can preferentially attach to different crystallographic planes of ice, and affect the mechanism of ice formation—or lack thereof—accordingly (Olijve et al. 2016; Haji-Akbari 2016).

3.4.2 Thermodynamics and Kinetics of Ice Formation in Pure Water

3.4.2.1 Thermodynamics of Ice Formation

In Sect. 3.2, a brief overview is provided on the basics of the thermodynamics of crystallization, and concepts such as melting point and triple point are introduced. Table 3.1 summarizes the thermodynamic properties of ice I and its corresponding liquid–solid transition. Ice I has a melting temperature of $T_m = 273.15$ K, and has an enthalpy of fusion of 1.436 kcal mol^{-1} at T_m. The gas–liquid–solid triple point of water is at 273.16 K and 61 Pa. Note that the triple point temperature is slightly higher than T_m due to the negative slope of the ice I–liquid coexistence line. Also, water has an unusually high melting point in comparison to similar molecules, a fact that has been attributed to the dominant role that hydrogen bonding plays in condensed phases of water.

3.4.2.2 Kinetics of Ice Formation: Nucleation and Growth

According to classical thermodynamics, a *supercooled* liquid, i.e., a liquid below its equilibrium melting temperature, is thermodynamically unstable and will eventually freeze into its respective crystal. But the fact that such a transformation is thermodynamically favored does not imply that it will occur within experimentally accessible timescales. Indeed, supercooled water—or any other supercooled liquid for that

Table 3.1 Thermodynamic and structural properties of hexagonal ice (Petrenko 1993)

Property	Value
Density	917 kg m^{-3}
Melting point	273.15 K
Latent heat of fusion	1.436 kcal mol^{-1}
Heat capacity	8.79 cal mol^{-1} K^{-1}
Thermal conductivity	0.234 W m^{-1} K^{-1}
Solid/liquid surface energy	33 mJ m^{-2}
Solid/vapor surface energy	109 mJ m^{-2}
Triple Point (ice I/liquid/gas)	273.16 K, 61 Pa
Dielectric permittivity	95

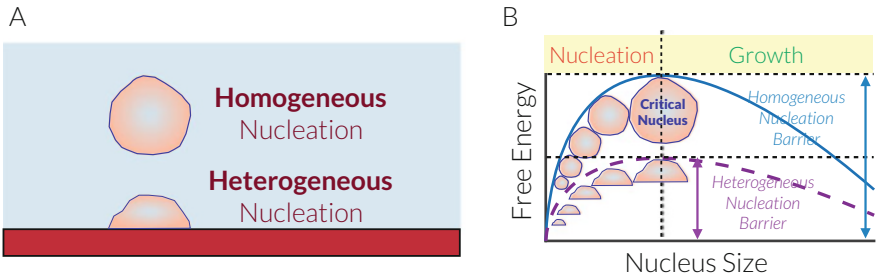

Fig. 3.4 (**a**) Ice can nucleate either homogeneously (e.g., in pure water in the absence of a facilitating surface) or heterogeneously in the vicinity of an interface. (**b**) Schematic free energy of the system as a function of nucleus size for both homogeneous and heterogeneous nucleation

matter—can remain liquid, sometimes for very long times. Such a delay arises from the fact that crystallization—like any other first-order phase transition—proceeds through a mechanism known as *nucleation and growth* (Fig. 3.4). Nucleation is an activated process and involves the formation of a sufficiently large crystalline nucleus within the supercooled liquid, while growth refers to the subsequent enlargement of that nucleus. The activated nature of nucleation arises from the free energetic penalty associated with the formation of a solid–liquid interface. This penalty, which exists due to structural mismatch between an ordered crystal and a disordered liquid, scales linearly with the surface area of the crystalline nucleus, and is eventually overcome by the thermodynamic driving force for crystallization, which scales linearly with the volume of the nucleus. For small nuclei, however, this surface contribution is dominant and makes nuclei that are smaller than a critical size thermodynamically unstable. This makes the formation of a critical nucleus a stochastic activated process unless its free energy of formation is comparable to thermal fluctuations in the system.

The qualitative argument provided above is made more rigorous in *classical nucleation theory (CNT)*. Proposed in the early twentieth century (Volmer and Flood 1934; Becker and Döring 1935), CNT is the most widely used theoretical framework for crystal nucleation (Oxtoby 1992). In the simplest variant of CNT, it is assumed that crystalline nucleus is spherical in shape, and the properties of the solid and the liquid are bulk-like and are not affected by the presence of an interface. The free energy of formation of a crystalline nucleus composed of N molecules will then be given by (Debenedetti 1996):

$$G(N) = -\frac{N|\Delta\mu|}{N_A} + \left(\frac{36\pi}{\rho_s^2}\right)^{1/3} \sigma_{ls} N^{2/3} \tag{3.3}$$

Here, $\Delta\mu$ is the chemical potential difference between the liquid and the solid, N_A is the Avogadro number, and ρ_s and σ_{ls} are the solid number density and the solid–liquid surface tension, respectively. Equation (3.3) has a maximum at:

$$N_c = \frac{\sigma_{ls}}{|\Delta\mu|}\left(\frac{32\pi}{3\rho_s^2}\right)^{2/3} \tag{3.4}$$

The free energy of formation for a nucleus with N_c molecules is called the *nucleation barrier* and is given by:

$$\Delta G_{nuc} = G(N_c) = \frac{N_c}{2N_A}|\Delta\mu| = \frac{16\pi\sigma_{ls}^3 N_A^2}{3\rho_s^2|\Delta\mu|^2} \tag{3.5}$$

Due to this non-monotonicity in $G(N)$, forming a critical nucleus is an uphill battle thermodynamically. Assuming that a steady-state nucleus size distribution is established at timescales much shorter than the nucleation time, it can be demonstrated that a fluctuation resulting in barrier crossing will have an occurrence probability proportional to $\exp[-\Delta G_{nuc}/kT]$ with k the Boltzmann constant. The *nucleation rate*, or the expected number of nucleation events per unit time per unit volume, will then be given by:

$$R = \frac{24\rho_{liq}DN_c^{3/2}}{l^2}\left(\frac{|\Delta\mu|}{6\pi kTN_c}\right)^{\frac{1}{2}}\exp\left[-\frac{\Delta G_{nuc}}{kT}\right] \tag{3.6}$$

with ρ_{liq} and D the density and the self-diffusivity of the liquid, and l the atomic jump distance in the liquid. Note that the stochastic nature of nucleation will imply that the nucleation time τ will be a stochastic random variable and will have a mean given by $\langle\tau\rangle = 1/(RV)$, with V the volume of the supercooled liquid. It is generally assumed that nucleation is a Poisson process[2] and nucleation time is exponentially distributed (Koop 2004). Upon the formation of a critical nucleus, however, there is no longer any thermodynamic resistance for its further growth, and the growth timescale is governed by the pace of structural relaxation in the system.

Depending on the magnitude of the nucleation barrier, either nucleation or growth can be the rate-limiting step in crystallization. When the nucleation barrier is very large, i.e., when $\Delta G_{nuc} \gg kT$, crystallization will be *nucleation limited* and nucleation times will be orders of magnitude larger than growth times. For $\Delta G_{nuc} \approx kT$, however, crystallization will be *growth limited* as a large number of nucleation events will occur simultaneously in the system, and the crystallization timescale will be determined by the intrinsic dynamics of the system, most importantly by its self-diffusivity.

In order to identify the conditions under which crystallization is nucleation limited or growth limited, it is first necessary to examine how $|\Delta\mu|$ and σ_{ls} change with thermodynamic variables such as temperature. In general, solid–liquid surface tension is extremely difficult to measure in the deeply supercooled regime, and even

[2]To be more precise, it is the number of nucleation events per unit time within an ensemble of independent nucleation experiments, e.g., isolated microdroplets, that is a Poisson process.

though it is known that σ_{ls} is an increasing function of temperature, its precise dependence on T is not known due to technical difficulties of measuring it far from equilibrium (Gŕańasy et al. 2002). $|\Delta\mu|$, however, can be rigorously calculated from integrating the equations of state of the supercooled liquid and the crystal:

$$|\Delta\mu| = T\int_{T}^{T_m} \frac{\left|h_{I_h} - h_{liq}\right|}{\overline{T}^2} d\overline{T} \tag{3.7}$$

with h_{I_h} and h_{liq} the molar enthalpies of ice I_h and the supercooled liquid, respectively. Assuming that molar enthalpies are not strong functions of temperature, it can be easily shown that:

$$\Delta\mu = \Delta h_m \left[1 - \frac{T}{T_m}\right] \tag{3.8}$$

where Δh_m is the enthalpy of fusion at T_m. Combining Eqs. (3.5) and (3.8) yields:

$$\frac{\Delta G_{nuc}}{kT} = \frac{16\pi\sigma_{ls}^3 N_A^2 T_m^2}{3kT\rho_s^2 \Delta h_m^2 (T_m - T)^2} = \frac{B}{kT(T - T_m)^2} \tag{3.9}$$

Therefore, the nucleation barrier depends on $\Delta T = T_m - T$, which is typically referred to as *the degree of supercooling*.[3] Equation (3.9) predicts that ΔG_{nuc} is a decreasing function of ΔT, an assertion that is generally true even if Eq. (3.8) is not valid. Therefore, nucleation rate should increase exponentially upon decreasing temperature. Such an increase in rate is, however, eventually offset by the slowdown of intrinsic dynamics at low temperatures. Assuming that transport properties such as self-diffusivity have an Arrhenius-type dependence[4] on temperature, i.e., $D \sim \exp[-E_a/kT]$, the overall crystallization rate will be given by:

$$R = A\ \exp\left\{-\frac{1}{kT}\left[\underbrace{E_a}_{\text{diffusion}} + \underbrace{\frac{B}{\Delta T^2}}_{\text{nucleation}}\right]\right\} \tag{3.10}$$

Therefore, nucleation-limited crystallization will occur at small supercoolings where the rate of increase in $\exp[-\Delta G_{nuc}/kT]$ is much faster than the slowdown in D.

[3] An alternative definition for the degree of supercooling is $\theta = T/T_m$. See Gianetti et al. (2016) for discussion.

[4] For strong liquids, D has an Arrhenius-like dependence on temperature. In fragile liquids, however, D drops much more abruptly as temperature decreases. Depending on the extent of supercooling water can be strong or fragile. In the nucleation-limited regime, i.e., at temperatures close to T_m, water behaves as a fragile liquid, while amorphous ices act as strong liquids. Therefore, it has been speculated that a fragile-to-strong transition occurs in the no man's land.

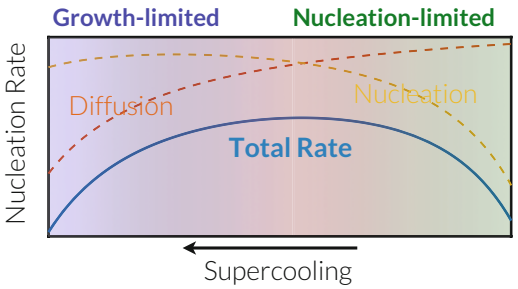

Fig. 3.5 Schematic representation of the dependence of the rate of ice nucleation on temperature. Nucleation- and growth-limited regimes are depicted in green and blue, respectively

Growth-limited crystallization, however, will take place under conditions at which Eq. (3.10) is dominated by the E_a/kT term, i.e., at large supercoolings. In the middle, there will always be a temperature at which the nucleation rate will be the largest. Figure 3.5 depicts the schematic dependence of nucleation rate on ΔT, with the nucleation- and growth-limited regimes depicted in green and blue, respectively.

The discussion presented so far only applies to *homogeneous nucleation* in which a critical nucleus forms in the absence of an external surface. In the case of water, barriers for homogeneous nucleation are so large that it can only occur at temperatures below ≈235 K, and is practically impossible for temperatures above –20 °C (Sanz et al. 2013). With extra care, water microdroplets can be supercooled for temperatures as low as 227 K (Sellberg et al. 2014). All our daily experience of freezing, therefore, involve *heterogeneous nucleation* in which an external surface facilitates freezing by decreasing nucleation barriers. There are a wide variety of materials that can heterogeneously nucleate ice, including mineral dust (Chen et al. 2008; Zimmermann et al. 2008; Hoose et al. 2010; Atkinson et al. 2013; Kiselev et al. 2017), volcanic ash (Schumann et al. 2011), soot (Jensen and Toon 1997; Chen et al. 2008; Hoose et al. 2010), organic materials (Wilson et al. 2015), ammonium sulfate particles (Hoose and Möhler 2012), and biological materials such as pollen and bacteria (Chen et al. 2008; Hoose et al. 2010; Joly et al. 2013; Wilson et al. 2015; O'Sullivan et al. 2015) and diatoms (Knopf et al. 2011). Interestingly biological materials are among the most potent ice-nucleating agents (Murray et al. 2012).

An extension of CNT for heterogeneous nucleation was formulated by Turnbull (1950), in which it is assumed that the crystalline nucleus is a spherical cap and its shape does not change during nucleation. According to CNT for heterogeneous nucleation, the nucleation barrier will be given by $\Delta G_{\text{nuc}}^{\text{het}} = f(\theta_c)\Delta G_{\text{nuc}}^{\text{homo}}$. Here, θ_c is the three-phase contact angle between the crystal, the supercooled liquid and the external surface, and $f(\theta_c) = \frac{1}{4}(1 - \cos\theta_c)^2(2 + \cos\theta_c)$ is called the *potency factor*. Note that whenever $\theta_c < \pi$, i.e., when the external surface has a higher propensity for the crystal than for the supercooled liquid, the barrier for heterogeneous nucleation will always be smaller than the barrier for homogeneous nucleation at the same temperature. Therefore, the temperature at which the nucleation rate becomes maximum increases in heterogeneous nucleation, but the overall qualitative picture depicted in Fig. 3.5 remains unchanged. Also, the nucleation rate in heterogeneous nucleation should be expressed as the number of nucleation events per time

per area, and nucleation time will have a mean given by $\langle \tau \rangle = 1/(RS)$ with S the total surface area of all ice-nucleating particles in the system. It is, however, usually possible to obtain an effective volumetric nucleation rate by accounting for the volumetric concentration of ice-nucleating particles, and the surface area of each such particle.

Another remarkable feature about heterogeneous nucleation is that it does not occur on solid-like surfaces only, but can also take place at a fluid–fluid interface. For instance, it has been demonstrated that amphiphilic alcohol monolayers (Gavish et al. 1990; Popovitz-Biro et al. 1994; Seeley and Seidler 2001) and terpenes (Rosinski 1980; Rosinski and Lecinski 1981; Rosinski et al. 1990) can facilitate ice nucleation. A more interesting possibility, which has been studied extensively both in experiments (Djikaev et al. 2002; Tabazadeh et al. 2002; Kuhn et al. 2011) and simulations (Gianetti et al. 2016; Vrbka and Jungwirth 2006; Pluhárová et al. 2010; Li et al. 2013b; Haji-Akbari et al. 2014; Haji-Akbari and Debenedetti 2017a), is that water–vapor interfaces can facilitate ice nucleation at their vicinity. This latter scenario is called *surface freezing* and has been predicted to become dominant in submicron microdroplets (Kuhn et al. 2011). Due to the difficulty of generating monodispersed submicron droplets, however, whether surface freezing occurs or not is still controversial (Sigurbjörnsson and Signorell 2008) and is regarded as one of the ten biggest open questions about ice and snow (Bartels-Rausch 2013). A detailed discussion of surface freezing can be found in an earlier review (Haji-Akbari and Debenedetti 2017b).

3.4.2.3 Ice Nucleation and Ice I Polytopes

As mentioned earlier, hexagonal ice is the thermodynamically stable form of ice I under ambient conditions, and the type of ice that forms at temperatures close to T_{m}. However, this does not necessarily imply that the crystalline nuclei that emerge during nucleation are exclusively hexagonal. Indeed, the ice that nucleates homogeneously at low temperatures (Dowell and Rinfret 1960; Mayer and Hallbrucker 1987; Kohl et al. 2000; Murray et al. 2005; Shilling et al. 2006) or in ultra-confined geometries (Johari 2005; Steytler et al. 1983; Morishige and Uematsu 2005; Morishige et al. 2009) is stacking disordered, with a considerable fraction of cubic stacks (Malkin et al. 2012; Amaya et al. 2017). If temperatures are sufficiently high, stacking disordered ice will eventually anneal to the thermodynamically stable hexagonal ice (Murray et al. 2005; Gainaru et al. 2018).

The fact that a liquid would nucleate into a thermodynamically metastable crystal is not surprising and has been observed in other systems (ten Wolde and Frenkel 1999). It has indeed been argued that if that metastable crystal has a lower solid–liquid surface tension than the thermodynamically stable crystal, it will be the first to nucleate in the liquid. The emerging nucleus will then nucleate the thermodynamically stable phase from within when it becomes sufficiently large (ten Wolde et al. 1996). This is typically called *Ostwald's step rule*, and stipulates that crystallization of a liquid into the thermodynamically stable crystal will usually occur in stages

(Van Santen 1984). Ostwald's step rule has been invoked to explain the formation of I_{sd} during ice nucleation (Takahashi 1982). It has, however, not been established whether I_c and I_{sd} have lower solid–liquid surface tensions than the thermodynamically stable hexagonal ice. Furthermore, the validity of Ostwald's step rule at a molecular level cannot be confirmed using existing experimental techniques due to their insufficient spatiotemporal resolution.

In recent decades, molecular simulations have shed more light on the molecular origin of stacking disorder in ice nucleation. Molecular simulations utilizing different water models and simulation techniques have indeed revealed the formation of stacking disordered ice during nucleation (Brukhno et al. 2008; Moore and Molinero 2010, 2011a, b; Johnston and Molinero 2012; Reinhardt and Doye 2012; Reinhardt et al. 2012; Haji-Akbari and Debenedetti 2015, 2017a; Lupi et al. 2017). In unbiased molecular dynamics simulations of the monoatomic water (mW) potential (Molinero and Moore 2009), a coarse-grained model of water, it has been observed that homogeneous nucleation in the deeply supercooled regime results in the formation of nuclei that are stacking disordered, and their fraction of cubic stacks increases when they become larger, eventually reaching a plateau of $\sim$60% (Moore and Molinero 2010, 2011a, b). The formation of I_{sd} is, however, not confined to mW and has been observed for atomistic models of water as well (Brukhno et al. 2008; Reinhardt et al. 2012; Haji-Akbari and Debenedetti 2015, 2017a).

So far, two distinct explanations have been proposed for the emergence of stacking disorder during ice nucleation. The first explanation is kinetic in nature, and was provided by Haji-Akbari and Debenedetti (2015), who utilized atomistic simulations and forward-flux sampling (FFS) (Allen et al. 2006) to compute the rate and explore the mechanism of homogeneous ice nucleation for TIP4P/Ice (Abascal et al. 2005), one of the most accurate atomistic models of water. They monitored the presence of HCs and DDCs, the topological building blocks of I_h and I_c, and observed that DDC-rich nuclei have smaller surface-to-volume ratios and are therefore more likely to grow and become post-critical. HC-rich nuclei, however, emerge mostly as a result of the attachment of new HCs to prismatic faces of existing HCs. The dominance of prismatic growth culminates in HC-rich nuclei that are composed of chains of hexagonal cages, and that have large surface-to-volume ratios. The fact that new HCs are added prismatically has a kinetic origin, and results in disfavoring HC-rich crystallites and favoring the formation of stacking disordered ice with a high fraction of cubic stacks. This mechanism has been confirmed in a later study utilizing a more accurate variant of the FFS technique (Haji-Akbari 2018). Computational studies of bulk ice also confirm that ice growth is the fastest at prismatic planes, presumably due to their higher surface energies (Seo et al. 2012; Rozmanov and Kusalik 2012).

The second explanation is thermodynamic in nature and was proposed by Lupi et al. (2017), who used molecular dynamics simulations and the aimless shooting method (Mullen et al. 2015) to compute the free energy landscape for homogeneous nucleation in the mW system, as a function of nucleus size and cubicity. They concluded that the entropy associated with mixing cubic and hexagonal layers makes stacking disordered nuclei more stable than their pure cubic and hexagonal

counterparts. This entropic contribution is proportional to the number of stacks, and scales as $N^{1/3}$, with N the number of water molecules in the nucleus. In bulk ice, i.e., for $N \to \infty$, this entropic contribution will be negligible in comparison to the free energy difference between I_c and I_h, which will scale as $O(N)$. For small nuclei with a few hundred water molecules, however, this entropic contribution will be significant and will decrease the nucleation barrier by enhancing the stability of stacking disordered nuclei. It is necessary to note that these explanations are not mutually exclusive, and the preference for stacking disordered ice is likely a consequence of both thermodynamic and kinetic effects.

3.4.2.4 Melting of Ice I: Gibbs–Thomson Equation and Recrystallization

Similar to freezing, melting of crystals, such as ice, is a first-order transition, proceeds through nucleation and growth, and can be delayed at temperatures higher than T_m for kinetic reasons. In other words, similar to liquid water that can be supercooled and remain liquid at temperatures below T_m, ice can also be *superheated* and remain crystalline at temperatures above T_m (Iglev et al. 2006). What is different about melting, however, is that every crystal has an intrinsic stability limit, i.e., a temperature above which it becomes mechanically unstable due to high-amplitude thermal vibrations of its constituent atoms and/or molecules (Lindemann 1910). Homogeneous nucleation of the liquid can, however, occur before this stability limit is reached, as confirmed in several experimental (Wang et al. 2012, 2015) and computational (Mochizuki et al. 2013; Samanta et al. 2014) studies. In reality, most crystals melt heterogeneously at temperatures that are only slightly higher than T_m and are thus much lower than this stability limit. Heterogeneous melting can be induced at external surfaces, or at internal defects such as grain boundaries. What is remarkable about heterogeneous melting is the ability of most external surfaces to destabilize crystals even at temperatures below T_m, resulting in the formation of a thin pre-melted quasi-liquid layer in their vicinity. This phenomenon—also known as *premelting*—has been extensively studied for ice (Dash et al. 1995; Bluhm et al. 2002; Sánchez et al. 2017) and other materials (Ronchi and Hiernaut 1996; Kristensen and Cotterill 1977) in recent decades. A crystal that is in contact with a surface that induces premelting cannot be superheated, as at any $T > T_m$, the pre-melted layer will immediately destabilize the bulk crystal at its vicinity and will result in its melting without a need to cross a nucleation barrier.

Considering the preponderance of surface premelting, superheating is not very common, and in order for a crystal to be superheated, it needs to be engulfed by surfaces that do not induce premelting. This can, for instance, be achieved by embedding nanocrystals of the target crystal within a matrix of a second crystal with a higher melting point, a method that has been used to superheat metals (Banhart et al. 2003) and Group IV elements such as germanium (Xu et al. 2006). Crystals that have been frozen within solutions with kinetic inhibitors such as antifreeze proteins can also be superheated, as such inhibitors can bind to crystalline

particles and provide the engulfment discussed above in an irregular manner. Therefore, the ice that forms in the presence of antifreeze proteins can be superheated (Knight and DeVries 1989; Celik et al. 2010; Cziko et al. 2014), a process that will be discussed in further detail in other chapters.

It is necessary to emphasize that confinement does not only affect the kinetics of melting, but can also impact its thermodynamics. For instance, the equilibrium melting temperature can change considerably for water entrapped in nanopores (Findenegg et al. 2008; Sliwinska-Bartkowiak et al. 2008; Moore et al. 2012). One of the most notable examples of how confinement can affect the thermodynamics of melting is the depression of equilibrium melting point for small crystalline particles. In order to understand the origin of this depression, consider a spherical ice particle of radius r, which, due to its surface curvature, will experience a heightened internal pressure. The pressure difference between the crystal interior and the surrounding liquid is called the *Laplace pressure* and can be estimated using the Young–Laplace equation (Chen et al. 2006):

$$\Delta P = \frac{2\sigma_{\mathrm{ls}}}{r} \tag{3.11}$$

This ΔP will increase the chemical potential of the crystal by $\Delta\mu = v_{\mathrm{ice}}\Delta P = 2\sigma_{\mathrm{ls}}/\rho_{\mathrm{ice}}r$ and will make it thermodynamically unstable at the bulk melting temperature T_{m}. Instead, thermodynamic equilibrium will be achieved at a lower temperature $T_{\mathrm{m}}(r)$ where this curvature-induced penalty is offset by the bulk thermodynamic driving force given by Eq. (3.8). It can be shown using simple thermodynamic reasoning that $T_{\mathrm{m}}(r)$ will be given by:

$$T_{\mathrm{m}}(r) = T_{\mathrm{m,bulk}} - \frac{2\sigma_{\mathrm{ls}}\,T_{\mathrm{m,bulk}}}{\rho_{\mathrm{s}}\,r\,\Delta h_{\mathrm{m}}} \tag{3.12}$$

Equation (3.12) is known as the *Gibbs–Thomson equation* (Jackson and McKenna 1990; Johari 1997). A similar argument can be made to obtain the depressed T_{m} for arbitrarily shaped surfaces (Johnson 1965; Jones 1974), including a spherical cap of radius r sitting on top of an ice-nucleating surface. A closely related equation is the *Kelvin equation*, which describes the dependence of the equilibrium vapor pressure of a droplet as a function of its size (Thomson 1872):

$$P(r) = P(\infty)\ \exp\left[\frac{2\sigma_{\mathrm{lv}}}{\rho_{\mathrm{l}}rkT}\right] \tag{3.13}$$

with $P\,(r)$ and $P\,(\infty)$ the equilibrium vapor pressure of a droplet of radius r, and bulk liquid, respectively, σ_{lv}, the liquid–vapor surface tension, and ρ_{l} the number density of the liquid.

An important consequence of this size-dependent stability is a phenomenon known as *recrystallization* or *Ostwald ripening* (Voorhees 1985), which refers to the growth of larger crystalline particles at the expense of smaller ones. This occurs

when the nucleation barrier is so small that a large number of post-critical nuclei emerge within the liquid. However, not all such nuclei will be identical in shape and size. Such polydispersity will generate a thermodynamic driving force for the growth of larger nuclei at the expense of smaller ones, which, as explained above, are less stable. One of the important functions of AFPs is to inhibit recrystallization, i.e., to prevent small crystalline nuclei—that are still larger than their surrounding nuclei—from growing any larger. This is important from a biological perspective since smaller crystallites are less harmful to biological cells (Knight et al. 1984). The ability of AFPs to prevent recrystallization will be discussed in detail in Chap. 7 of Vol. 2.

3.4.2.5 Thermal Hysteresis

Nucleation is, in essence, an out-of-equilibrium process in which a thermodynamically metastable system, such as a supercooled liquid, turns into a thermodynamically stable structure, such as a crystal. Therefore, when the coexistence line is crossed, e.g., by cooling a liquid, freezing does not occur immediately. Instead, the system remains in the metastable supercooled state until nucleation occurs. However, when nucleation is complete, the system reaches thermodynamic equilibrium, and remains there until the coexistence line is crossed in the opposite direction. Therefore, the behavior of a system that crosses a coexistence line depends on the direction of such crossing. This is known as *hysteresis* and is an important feature of all first-order phase transitions, including crystallization. As explained in Sect. 3.4.2, hysteresis can occur for both ice formation and ice melting, but is less common in the case of melting. An important manifestation of this is *thermal hysteresis* in biological systems, which refers to a situation in which a biological solution can exist as a liquid at temperatures below T_m (Finger and Bischof 2018) or as a solid at temperatures above T_m (Knight and DeVries 1989). In other words, at finite timescales, temperature is not sufficient for determining whether a system is frozen or not, and the system might behave differently based on its initial state and processing history. One measure of an AFP's potency is its ability to induce the largest possible thermal hysteresis, which will enable cells and/or organisms to survive freezing at lower temperatures.

3.4.3 Ice Formation in Solutions

So far, only the thermodynamics and kinetics of ice formation in pure water has been discussed. Biological water, however, is never pure, and in order to explore freezing in biological systems, it is important to understand how soluble impurities affect ice formation. The conceptual approach for analyzing freezing in aqueous solutions will depend on whether any of the solutes participates in the thermodynamic stable form of the aqueous crystal. Most solutes are excluded from the crystal, and therefore the

freezing of the corresponding solution results in the formation of pure ice I. As mentioned in Sect. 3.3.2, however, there are notable exceptions to this rule including aqueous solutions of small gaseous molecules that can crystallize into gas hydrates (Maslin et al. 2010; Knott et al. 2012). Here, the focus will be on the former scenario, i.e., on solutes that do not participate in the ice structure, and on their impact on the thermodynamics and kinetics of freezing.

3.4.3.1 Thermodynamics of Ice Formation in Solutions

The effect of soluble entities on the thermodynamics of ice formation is well understood, and is discussed in detail in all standard thermodynamics textbooks. In summary, adding a solute to water results in a decrease in its chemical potential given by:

$$\mu_{\mathrm{w,liq}}\left(T,P,x_{\mathrm{w,liq}}\right)=\mu^{0}_{\mathrm{w,liq}}(T,P)+RT\ln a_{\mathrm{w,liq}} \tag{3.14}$$

Here, $x_{\mathrm{w,liq}}$ is the mole fraction of water and $a_{\mathrm{w,liq}}<1$ is a dimensionless quantity known as *activity*. As mentioned earlier, thermodynamic coexistence is achieved when the chemical potentials of water in the liquid and the crystal become identical. Assuming that the solute does not participate in the thermodynamically stable crystal structure, the condition for thermodynamic coexistence between the solution and ice I will be given by:

$$\ln a_{\mathrm{w,liq}}(T_{\mathrm{m}})=\frac{\mu^{0}_{\mathrm{w,ice}}(T_{\mathrm{m}},P)-\mu^{0}_{\mathrm{w,liq}}(T_{\mathrm{m}},P)}{RT_{\mathrm{m}}}=-\frac{|\Delta\mu|}{RT_{\mathrm{m}}} \tag{3.15}$$

Since $a_{\mathrm{w,liq}}<1$, Eq. (3.15) can only be satisfied if $T_{\mathrm{m}}<T_{\mathrm{m}}^{\mathrm{pure}}$. This decrease in equilibrium freezing temperature is typically referred to as *freezing point depression*, which is defined as $\Delta T_{\mathrm{m}}\coloneqq T_{\mathrm{m}}^{\mathrm{pure}}-T_{\mathrm{m}}(x_{\mathrm{w}})$. Assuming the availability of $|\Delta\mu(T)|$, which can be obtained by integrating the equation of state, and the activity data versus temperature, which can, for instance, be readily obtained from vapor pressure—or fugacity—measurements, the depressed freezing point can be accurately calculated from Eq. (3.15). A simpler approach can, however, be employed for dilute solutions, i.e., solutions in which x_{S}, the total mole fraction of *all* solutes in the system, is much smaller than unity, i.e., when $x_{\mathrm{S}}\ll 1$. Under such circumstances, water activity will approach its mole fraction, and its chemical potential can be expressed as:

$$\begin{aligned}\mu_{\mathrm{w,liq}}\left(T,P,x_{\mathrm{w,liq}}\right)&=\mu^{0}_{\mathrm{w,liq}}(T,P)+RT\ln\left(1-x_{\mathrm{S}}\right)\\&\overset{x_{\mathrm{S}}\ll 1}{\approx}\mu^{0}_{\mathrm{w,liq}}(T,P)-x_{\mathrm{S}}RT\end{aligned} \tag{3.16}$$

Combining Eqs. (3.8) with Eqs. (3.15 and 3.16) yields:

$$T_{\mathrm{m}}(x_{\mathrm{S}}) = \frac{T_{\mathrm{m}}^{\mathrm{pure}}}{1+\frac{x_{\mathrm{S}} R T_{\mathrm{m}}^{\mathrm{pure}}}{\Delta h_{\mathrm{m}}}} \approx T_{\mathrm{m}}^{\mathrm{pure}} \left[1 - \frac{x_{\mathrm{S}} R T_{\mathrm{m}}^{\mathrm{pure}}}{\Delta h_{\mathrm{m}}}\right] \tag{3.17}$$

Therefore, freezing point depression in dilute solutions is a *colligative property* as it only depends on the overall molal concentration of the solutes and not on their chemical identities. Other notable colligative properties include vapor pressure depression, boiling point elevation, and osmotic pressure. Due to their relatively large molar masses, aqueous solutions of most biomolecules can be usually considered dilute, and Eq. (3.17) can usually be used for computing ΔT_{m}.

3.4.3.2 Kinetics of Ice Formation in Solutions

The presence of solutes in liquid water will alter its molecular structure, such as its hydrogen bond network. Such changes will inevitably affect the kinetics—and possibly the mechanism—of ice nucleation, and considering the out-of-equilibrium nature of nucleation and its strong sensitivity to even modest changes in thermodynamic properties, it is not a priori clear how the nucleation kinetics will be affected by the identities and concentrations of the corresponding solutes. Even if we assume the validity of the classical nucleation theory, it is not trivial to determine how properties such as solid–liquid surface tension will depend on solute concentration. The situation is even more hopeless in the case of heterogeneous nucleation, since an ice-nucleating surface can interact differently with water molecules and the solutes, and such differences can induce compositional anisotropies that can, in turn, affect the kinetics and mechanism of ice nucleation in nontrivial ways.

Despite these complexities, there seems to be overwhelming experimental evidence for the colligative nature of nucleation kinetics. In 1977, Kanno and Angel discovered that the amount of decrease in the kinetic freezing temperature[5] of an aqueous alkali halide solution is a colligative property and depends on cation concentration only (Kanno and Angell 1977). This idea was later generalized in the pioneering work of Koop et al. (2000) who studied sixteen different aqueous solutions, and demonstrated that water activity is sufficient for predicting the nucleation kinetics, irrespective of the identity of the solute. The qualitative argument for this empirical observation is that water activity is a proxy for how much its hydrogen bond network is perturbed in the presence of solute(s). This empirical framework is known as the *activity shift model* and works remarkably well for most simple solutes. Small deviations from it, however, have been observed in several systems (Swanson 2009; Knopf and Rigg 2011). Antifreeze proteins are among the most remarkable example of solutes that deviate from this colligative picture, resulting in kinetic suppressions considerably larger than what would otherwise be expected from their concentrations (Dolev et al. 2016; Olijve et al. 2016; Haji-

[5]Here, the kinetic freezing temperature refers to the highest temperature at which freezing occurs within the observation timescale of an experiment.

Akbari 2016). The activity shift model was originally proposed for homogeneous nucleation. Interestingly, the kinetics of heterogeneous nucleation has also been shown to follow the activity shift model (Zobrist et al. 2008; Wilson and Haymet 2009; Knopf and Alpert 2013; Zeng et al. 2015) with minor deviations also reported in some systems (Cantrell and Robinson 2006).

Despite its success in predicting the kinetics of ice nucleation in aqueous solutions, the activity shift model does not provide any information about how the nucleation mechanism is affected by a solute. For instance, the presence of soluble impurities has been shown to affect polymorph selection (i.e., the ratio of cubic to hexagonal ice) in deeply supercooled water (Murray and Bertram 2007; Murray 2008). In addition, there is a wide gap in our understanding of when and why the activity shift model is violated, and studying such violations can be a potent area of research.

3.4.3.3 Solute Exclusion and Its Consequences

As mentioned above, most aqueous solutions crystallize into ice I, and their constituent solutes do not participate in the crystal structure. This results in a phenomenon known as *solute exclusion* or *solute rejection* in which the freezing of an aqueous solution results in the formation of ice crystals that coexist with regions composed of more concentrated—and possibly saturated—aqueous solutions. Solute rejection has very important consequences in biological systems. Not only such concentrated regions can be toxic simply due to their high solute concentrations, but there will also be a steep osmotic gradient between them and less concentrated solutions, e.g., in the cytoplasm. Such a gradient will induce a strong water flow, which can, in turn, exert mechanical damage to cell membranes. This *osmotic shock* scenario is thought to be an important mechanism of ice toxicity. Interestingly, osmosis-induced ice toxicity usually occurs when freezing is extracellular, in which case water flow will be from the cytoplasm to the extracellular region (Muldrew and McGann 1990, 1994).

3.5 Amorphous Ices

The focus of Sect. 3.4 was to discuss water's equilibrium behavior at ambient pressures and subfreezing temperatures. This section, however, will deal with out-of-equilibrium glassy states of water that share the molecular structure of liquid water but, due to their slow dynamics, exhibit mechanical properties of a solid. Like most other liquids, water can be turned into a glass via a number of means including—but not limited to—rapidly quenching the liquid. Such kinetically arrested states are known as *amorphous ices* and the process employed for making them is called *vitrification*. Amorphous ices can avoid crystallization within experimentally accessible timescales as long as they are kept at temperatures below the glass transition

temperature T_g, which, for liquid water, is ~136 K at ambient pressures (Fuentes-Landete et al. 2015). Note that crystallization can be delayed for relatively long times even at temperatures slightly above T_g, since in order for the viscous water to crystallize, a large number of molecular rearrangements will still need to occur. At ambient pressures, for instance, crystallization will become sufficiently fast to be considered instantaneous at or above $T_x \sim 150$ K (Fuentes-Landete et al. 2015). In the interstellar space, temperatures are usually much lower than T_g. Consequently, amorphous ice is the predominant form of ice in the outer space (Mitchell et al. 2017). This is in contrast to earth where subfreezing temperatures are much higher than T_x, and therefore it is the crystalline ice that is prevalent.

Amorphous ices are out of equilibrium in nature, and their properties depend heavily on their processing history. Consequently, classifying amorphous ices based on their structural and physical properties is not trivial, and there are a large number of names and acronyms currently in use in the literature to describe different types of amorphous ices. In terms of processing history, amorphous ices are broadly classified into five categories as depicted in Fig. 3.6a. Historically, glassy water was first obtained through a process in which water vapor was physically deposited onto the surface of a cold copper rod at temperatures below 130 K (Burton and Oliver 1935). Vapor-deposited amorphous ice is typically referred to as *amorphous solid water* (*ASW*), is usually very porous, and can have densities as low as 0.3 g cm^{-3}. Upon annealing, however, ASW can undergo pore collapse and its specific surface area can decrease by as much as 2–3 orders of magnitude (Baragiola 2003). Vapor deposition is the primary mechanism of vitrification in comets and in the interstellar space (Mayer and Pletzer 1986).

Hyperquenched glassy water (*HGW*) is a type of glassy water obtained via rapid quenching of water microdroplets, which are then deposited onto the surface of a cold "cryoplate" (Mayer 1985). In order for HGW to form, the quenching rate must be ~10^6 K/s or higher. *High-density amorphous ice (HDA)* is another type of amorphous ice, obtained via pressure melting of hexagonal ice, e.g., at 77 K and 1.0 GPa (Mishima et al. 1984). Annealing HDA at low and high pressures results in the formation of *low-density amorphous ice* (*LDA*) (Mishima et al. 1985) and *very high-density amorphous ice* (*VHDA*) (Loerting et al. 2001), respectively.

Three of these five classes, i.e., ASW, HGW, and LDA, are low-density amorphous ices, and share the same molecular structure. The local environment of each water molecule within LDA (and other related low-density glasses) is remarkably similar to that of ice I in the sense that each molecule has four tetrahedrally arranged nearest neighbors and there is a clear separation between the first and second hydration shells, as manifested in the oxygen–oxygen radial distribution functions depicted in Fig. 3.6b. Unlike ice I, however, LDA lacks long-range translational order. The local tetrahedrality of the first hydration shell is disrupted in both HDA and VHDA in which the first hydration shell is penetrated by one and two water molecules from the second shell, respectively, as evident from the emergence of a weak second peak at ≈0.4 nm in HDA (Finney et al. 2002b) and ≈0.35 nm in VHDA (Finney et al. 2002a). Therefore, from a structural perspective, amorphous ices are classified into three categories: LDA, HDA, and VHDA.

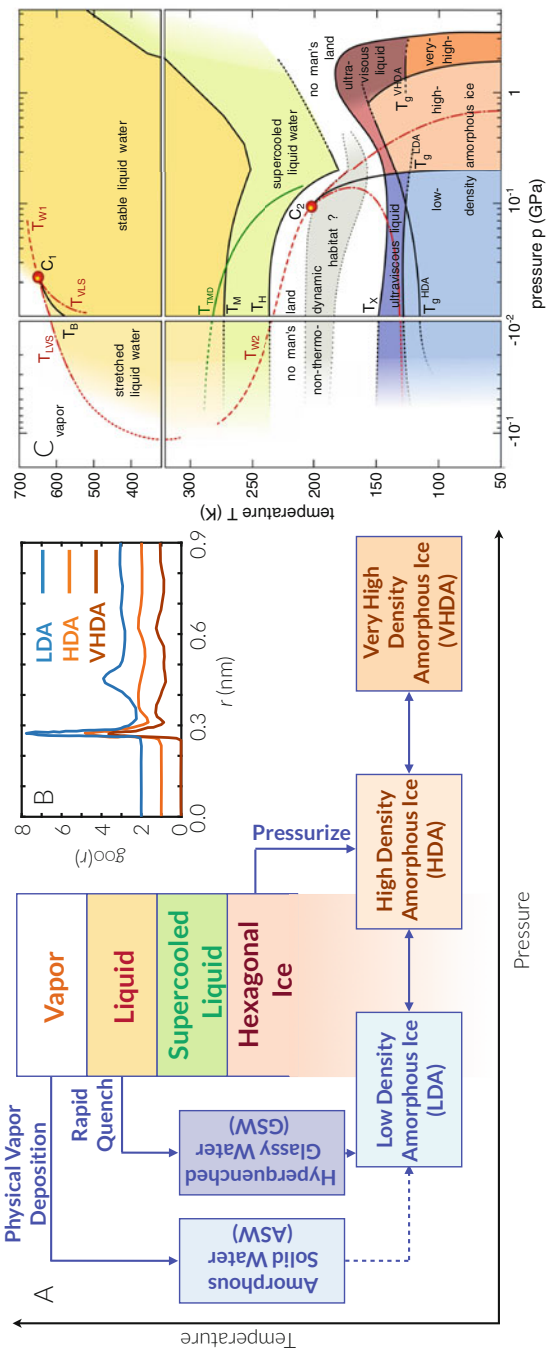

Fig. 3.6 Metastable phase diagram of liquid water. (**a**) Procedures for preparing different types of amorphous ices, adapted and simplified from Fig. 8 of Fuentes-Landete et al. (2015). (**b**) O–O radial distribution functions for LDA, HDA, and VHDA adapted and replotted from Finney et al. (2006). (**c**) Metastable phase diagram of liquid water (Reproduced from Amann-Winkel et al. 2016)

Another remarkable feature of these three structurally distinct amorphous ices is that they can be reversibly (Winkel et al. 2008) transformed into one another without crystallizing. The transition from LDA to the other two types is particularly sharp and is believed to be first order in nature (Finney et al. 2002a; Lemke et al. 2017). The notion that a material can exist in multiple amorphous phases that can reversibly transform into one another via first-order transitions is called *polyamorphism*. Studying glassy water polyamorphism is particularly interesting in the context of low-temperature water anomalies (Ball 2008; Brovchenko and Oleinikova 2008). There are a large number of such anomalies in the literature, including density maximum at 4 °C, isothermal compressibility minimum 46 °C and isobaric heat capacity minimum at and 35 °C. The origin of such anomalies are, however, yet to be fully understood, and four distinct scenarios have been proposed to explain them (Stanley and Teixeira 1980; Stanley et al. 1981; Speedy 1982; Poole et al. 1992; Sastry et al. 1996; Angell 2008; Stokely et al. 2009). Among these scenarios, the liquid–liquid transition hypothesis (Poole et al. 1992) is inspired by amorphous ice polyamorphism and attributes water anomalies to the existence of two distinct liquids in the supercooled regime, namely the low-density liquid (LDL) and the high-density liquid (HDL). According to this hypothesis, HDL and LDL are separated by a coexistence line that culminates in a liquid–liquid critical point (LLCP), and are the liquid counterparts of LDA and HDA, respectively. As can be seen in the metastable phase diagram of supercooled water in Fig. 3.6c (Amann-Winkel et al. 2016), the predicted liquid–liquid critical point is located below the homogeneous nucleation line and is therefore not accessible to existing experimental techniques. In recent years, there have been numerous experimental efforts to access this LLCP (Sellberg et al. 2014; Laksmono et al. 2015). Also, molecular simulations have been extensively utilized to understand liquid–liquid transition in water (Poole et al. 1992; Errington and Debenedetti 2001; Sastry et al. 1996; Palmer et al. 2014, 2018a) and other tetrahedral liquids (Saika-Voivod et al. 2000; Sastry and Angell 2003; Xu et al. 2005; Smallenburg et al. 2014). The topic of liquid–liquid transition in supercooled water is, however, far from resolved and is an active area of research (Palmer et al. 2018b).

Due to their metastable nature, amorphous ices should, in principle, crystallize at sufficiently long times. Crystallization, however, becomes practically implausible below T_g, and only becomes instantaneous at temperatures considerably higher than T_g. The process in which an amorphous solid turns into a crystal is called *devitrification* or *recrystallization*. Note that the general meaning of the term "recrystallization" is already introduced in Sect. 3.4.2. Crystallization within a glass is a growth-limited process resulting in the formation of a large number of nuclei, and therefore falls into the general framework of recrystallization introduced in Sect. 3.4.2.

Different amorphous ices can freeze into different crystalline phases. LDA crystallizes within experimentally accessible timescales at around 150 K and transforms into stacking disordered ice with a large fraction of cubic stacks (Johari et al. 1996; Johari 1998). High-density amorphous ices, however, crystallize into other ice polymorphs depending on pressure and processing history. For instance, HDA has been shown to crystallize into ice VII and ice VIII (Hemley et al. 1989), and ice IX

(Seidl et al. 2013). VHDA, however, can transform into a wide variety of ice polymorphs at different pressures (Klotz et al. 2005). Amorphous ices can also be directly transformed into liquid water if they are heated so quickly that crystallization is avoided. The heating rates needed for this to occur are, however, around two orders of magnitude larger than the cooling rates needed for vitrification.

Similar to pure water, rapid quenching of an aqueous solution can result in the formation of an amorphous solid. As outlined in Sect. 3.4.3, the presence of solutes results in melting point depression, and a considerable decline in the nucleation rate. Meanwhile, aqueous solutions usually have higher viscosities in comparison to pure liquid, and their viscosities are stronger functions of temperature (Angell 2002). This deceleration of dynamics can become very pronounced in concentrated aqueous solutions to the extent that their T_g can considerably exceed that of pure water. For instance, concentrated divalent electrolytic solutions such as $Mg(NO_3)_2$ and $Ca(NO_3)_2$ can have T_g's that are tens of degrees Kelvin higher than that of pure water (Angell and Sare 1970), and aqueous solutions of sugars such as trehalose can have T_g's at or above room temperature (Green and Angell 1989). For most solutes, however, the extent of increase in T_g is not that large, but it can be generally stated that aqueous solutions have lower T_m's and higher T_g's. Consequently, homogeneous ice nucleation can occur over a narrower range of temperatures. This will imply that vitrifying an aqueous solution can be achieved at cooling rates considerably lower than what would be needed for vitrifying pure water. Similarly, it will be easier to bypass crystallization during the thawing of such glasses, as the required heating rates will also be considerably lower.

3.5.1 Biological Applications of Vitrification

Vitrification is, in essence, a process in which the liquid is kinetically arrested without considerable change to its microscopic structure. Therefore, whenever a biological cell is vitrified, its structure and the spatial distribution of its composition remain unchanged, unlike freezing that can damage it through a number of means, such as volumetric expansion, solute exclusion, and osmotic shock. Vitrification is therefore of considerable interest in *cryopreservation* applications (Fahy et al. 1984). Vitrified cells and tissues can, in principle, be preserved for years, if not decades, and considering that biological cells are composed of concentrated aqueous solutions of electrolytes, carbohydrates, and other biomolecules, they can be vitrified (and thawed) at considerably lower cooling (heating) rates in comparison to what will be needed for pure water. Yet, it is still difficult to vitrify entire tissues and organs due to possible heat transfer limitations. In other words, when a tissue or organ is rapidly cooled, its interior will be at a higher temperature than its surface at all times, and such temperature differences can result in the freezing of the interior while the surface is being vitrified. A similar problem can arise during thawing, and the tissue or organ can freeze from within due to inadequate heat transfer. Therefore, vitrification is generally used for preserving individual cells, such as sperms (Isachenko

et al. 2004), oocytes (Kuwayama et al. 2005; Cobo et al. 2008) and embryos (Rall and Fahy 1985; Rall 1987), or small tissues, such as cryo-electron microscopy specimen (Dubochet et al. 1988).

3.6 Conclusions

Water is a material that exhibits numerous anomalies, and as discussed in detail in this chapter, its crystallization is also anomalous in many different ways. In particular, water can form a large number of crystalline polymorphs, some of which are less dense than the liquid water at coexistence. In all these ice polymorphs, each water molecule is hydrogen bonded to four of its neighbors, with two as a proton donor, and two as a proton acceptor. The polymorph of ice that forms under ambient pressures is ice I, which is a layered structure in which each water molecule has four neighbors within its first hydration shell. Ice I has two stacking variants—or polytopes—known as hexagonal (I_h) and cubic (I_c) ice. Hexagonal ice is the thermodynamically stable polytope, and is the form that emerges upon freezing under physiologically relevant conditions. Structurally, I_h is anisotropic and has three major crystallographic planes with differing surface energies. Cubic ice, which is structurally less anisotropic, is metastable and only becomes relevant during crystallization at very low temperatures.

As a first-order phase transition, ice formation proceeds through a nucleation and growth mechanism, and can occur both homogeneously and heterogeneously. At temperatures close to T_m, the thermodynamic driving force for crystallization is small, and freezing is nucleation-limited. At deep supercoolings, however, nucleation becomes almost instantaneous and crystallization becomes growth-limited. What is particularly interesting about ice I is that its homogeneous nucleation can be delayed for temperatures as low as 235 K. Freezing of liquid water into ice is therefore primarily heterogeneous under physiologically relevant conditions.

Freezing is generally slower in aqueous solutions, in comparison to pure water. Not only the thermodynamic freezing temperature is depressed in the presence of soluble impurities, but also the nucleation rate decreases considerably. For most solutions, the deceleration of nucleation kinetics can be predicted using the activity shift model, which is based on the empirical observation that solutions with identical water activities will freeze at the same rate at any given temperature.

Finally, water can be transformed into an amorphous solid via a number of means, including rapid quenching of the liquid, or depositing water vapor onto the surface of a cold substrate. Such glassy states are known as amorphous ices, and exhibit the mechanical properties of a solid despite being structurally liquid-like. Amorphous ices form during vitrification, which is widely used in cryopreservation applications.

Acknowledgments A.H.-A. gratefully acknowledges the support of the National Science Foundation CAREER Award (Grant No. CBET-1751971).

References

Abascal JLF, Sanz E, Fernández RG, Vega C (2005) A potential model for the study of ices and amorphous water: TIP4P/Ice. J Chem Phys 122:234511
Algara-Siller G, Lehtinen O, Wang F, Nair R, Kaiser U, Wu H, Geim A, Grigorieva I (2015) Square ice in graphene nanocapillaries. Nature 519:443
Allen PB (2010) Interpreting the 4-index notation for hexagonal systems. arXiv preprint arXiv:1006.2842
Allen RJ, Frenkel D, ten Wolde PR (2006) Forward flux sampling type schemes for simulating rare events: efficiency analysis. J Chem Phys 124:194111
Amann-Winkel K, Böhmer R, Fujara F, Gainaru C, Geil B, Loerting T (2016) Colloquium: water's controversial glass transitions. Rev Mod Phys 88:011002
Amaya AJ, Pathak H, Modak VP, Laksmono H, Loh ND, Sellberg JA, Sierra RG, McQueen TA, Hayes MJ, Williams GJ et al (2017) How cubic can ice be? J Phys Chem Lett 8:3216–3222
Angell C (2002) Liquid fragility and the glass transition in water and aqueous solutions. Chem Rev 102(8):2627–2650
Angell CA (2008) Insights into phases of liquid water from study of its unusual glass-forming properties. Science 319:582–587
Angell C, Sare E (1970) Glass-forming composition regions and glass transition temperatures for aqueous electrolyte solutions. J Chem Phys 52:1058–1068
Arbuckle W (1986) Development of the ice cream industry. In: Ice cream. Springer, Boston, MA, pp 1–8
Atkinson JD, Murray BJ, Woodhouse MT, Whale TF, Baustian J, Carslaw KS, Dobbie S, O'Sullivan D, Malkin TL (2013) The importance of feldspar for ice nucleation by mineral dust in mixed-phase clouds. Nature 498:355–358
Bai J, Wang J, Zeng XC (2006) Multiwalled ice helixes and ice nanotubes. Proc Natl Acad Sci U S A 103:19664–19667
Bai J, Angell CA, Zeng XC (2010) Guest-free monolayer clathrate and its coexistence with two-dimensional high-density ice. Proc Natl Acad Sci U S A 107:5718–5722
Baker MB (1997) Cloud microphysics and climate. Science 276:1072–1078
Ball P (2008) Water: water—an enduring mystery. Nature 452:291
Banhart F, Hernandez E, Terrones M (2003) Extreme superheating and supercooling of encapsulated metals in fullerene-like shells. Phys Rev Lett 90(18):185502
Baragiola R (2003) Water in confining geometries. Springer, Berlin, p 359
Barati Farimani A, Aluru NR (2016) Existence of multiple phases of water at nanotube interfaces. J Phys Chem C 120:23763–23771
Bartels-Rausch T (2013) Chemistry: ten things we need to know about ice and snow. Nature 494:27–29
Becker R, Döring W (1935) Kinetische behandlung der keimbildung in übersättigten dämpfen. Ann Phys 416:719–752
Beltaos S, Prowse T (2009) River-ice hydrology in a shrinking cryosphere. Hydrol Process 23:122–144
Bernal J, Fowler R (1933) A theory of water and ionic solution, with particular reference to hydrogen and hydroxyl ions. J Chem Phys 1:515–548
Bluhm H, Ogletree DF, Fadley CS, Hussain Z, Salmeron M (2002) The premelting of ice studied with photoelectron spectroscopy. J Phys Condens Matter 14:L227
Bridgman PW (1912) Water, in the liquid and five solid forms, under pressure. Proc Am Acad Arts Sci 47:441–558
Brovchenko I, Oleinikova A (2008) Multiple phases of liquid water. ChemPhysChem 9:2660–2675
Brukhno AV, Anwar J, Davidchack R, Hande R (2008) Challenges in molecular simulation of homogeneous ice nucleation. J Phys Condens Matter 20:494243

Brygoo S, Henry E, Loubeyre P, Eggert J, Koenig M, Loupias B, Benuzzi-Mounaix A, Le Gloahec MR (2007) Laser-shock compression of diamond and evidence of a negative-slope melting curve. Nat Mater 6:274

Burton E, Oliver W (1935) X-ray diffraction patterns of ice. Nature 135:505

Cantrell W, Robinson C (2006) Heterogeneous freezing of ammonium sulfate and sodium chloride solutions by long chain alcohols. Geophys Res Lett 33:L07802

Carslaw KS, Harrison RG, Kirkby J (2002) Cosmic rays, clouds, and climate. Science 298:1732–1737

Celik Y, Graham LA, Mok Y-F, Bar M, Davies PL, Braslavsky I (2010) Superheating of ice crystals in antifreeze protein solutions. Proc Natl Acad Sci U S A 107:5423–5428

Chamberlain EJ, Gow AJ (1979) Effect of freezing and thawing on the permeability and structure of soils. Eng Geol 13:73–92

Chen T, Chiu M-S, Weng C-N (2006) Derivation of the generalized Young-Laplace equation of curved interfaces in nanoscaled solids. J Appl Phys 100(7):074308

Chen J-P, Hazra A, Levin Z (2008) Parameterizing ice nucleation rates using contact angle and activation energy derived from laboratory data. Atmos Chem Phys 8:7431–7449

Chen J, Schusteritsch G, Pickard CJ, Salzmann CG, Michaelides A (2016) Two dimensional ice from first principles: structures and phase transitions. Phys Rev Lett 116:025501

Chen J, Schusteritsch G, Pickard CJ, Salzmann CG, Michaelides A (2017) Double-layer ice from first principles. Phys Rev B 95:094121

Cobo A, Kuwayama M, Pérez S, Ruiz A, Pellicer A, Remohí J (2008) Comparison of concomitant outcome achieved with fresh and cryopreserved donor oocytes vitrified by the cryotop method. Fertil Steril 89:1657–1664

Cockburn A, Cockburn E, Reyman TA (1998) Mummies, disease and ancient cultures. Cambridge University Press, London

Corsetti F, Matthews P, Artacho E (2016) Structural and configurational properties of nanoconfined monolayer ice from first principles. Sci Rep 6:18651

Cziko PA, DeVries AL, Evans CW, Cheng C-HC (2014) Antifreeze protein-induced superheating of ice inside Antarctic notothenioid fishes inhibits melting during summer warming. Proc Natl Acad Sci USA 111:14583–14588

Damasceno PF, Engel M, Glotzer SC (2012) Predictive self-assembly of polyhedra into complex structures. Science 337:453–457

Dash J, Fu H, Wettlaufer J (1995) The premelting of ice and its environmental consequences. Rep Prog Phys 58(1):115

Debenedetti PG (1996) Metastable liquids: concepts and principles. Princeton University Press, Princeton, NJ

Debenedetti PG (2003) Supercooled and glassy water. J Phys Condens Matter 15:R1669

del Rosso L, Celli M, Ulivi L (2016a) New porous water ice metastable at atmospheric pressure obtained by emptying a hydrogen-filled ice. Nat Commun 7:13394

del Rosso L, Grazzi F, Celli M, Colognesi D, Garcia-Sakai V, Ulivi L (2016b) Refined structure of metastable ice XVII from neutron diffraction measurements. J Phys Chem C 120 (47):26955–26959

Djikaev Y, Tabazadeh A, Hamill P, Reiss H (2002) Thermodynamic conditions for the surface-stimulated crystallization of atmospheric droplets. J Phys Chem A 106(43):10247–10253

Dolev MB, Braslavsky I, Davies PL (2016) Ice-binding proteins and their function. Annu Rev Biochem 85:515–542

Dowell LG, Rinfret AP (1960) Low-temperature forms of ice as studied by X-ray diffraction. Nature 188:1144

Dubochet J, Adrian M, Chang J-J, Homo J-C, Lepault J, McDowall AW, Schultz P (1988) Cryo-electron microscopy of vitrified specimens. Q Rev Biophys 21:129–228

Engel EA, Monserrat B, Needs RJ (2015) Anharmonic nuclear motion and the relative stability of hexagonal and cubic ice. Phys Rev X 5:021033

Errington JR, Debenedetti PG (2001) Relationship between structural order and the anomalies of liquid water. Nature 409(6818):318
Fahy GM, MacFarlane D, Angell C, Meryman H (1984) Vitrification as an approach to cryopreservation. Cryobiology 21(4):407–426
Falenty A, Hansen TC, Kuhs WF (2014) Formation and properties of ice XVI obtained by emptying a type sII clathrate hydrate. Nature 516:231
Findenegg GH, Jähnert S, Akcakayiran D, Schreiber A (2008) Freezing and melting of water confined in silica nanopores. ChemPhysChem 9:2651–2659
Finger EB, Bischof JC (2018) Cryopreservation by vitrification: a promising approach for transplant organ banking. Curr Opin Organ Tran 23(3):353–360
Finney J, Bowron D, Soper A, Loerting T, Mayer E, Hallbrucker A (2002a) Structure of a new dense amorphous ice. Phys Rev Lett 89(20):205503
Finney J, Hallbrucker A, Kohl I, Soper A, Bowron D (2002b) Structures of high and low density amorphous ice by neutron diffraction. Phys Rev Lett 88(22):225503
Finney J, Hallbrucker A, Kohl I, Loerting T, Soper A (2006) The local and intermediate range structures of the five amorphous ices at 80 K and ambient pressure: a Faber-Ziman and Bhatia-Thornton analysis. J Chem Phys 125:194502
Fletcher NH (1970) Other forms of ice. In: Cambridge monographs on physics. Cambridge University Press, Cambridge, pp 49–72
Fowler LD, Randall DA, Rutledge SA (1996) Liquid and ice cloud microphysics in the CSU general circulation model. Part 1: Model description and simulated microphysical processes. J Clim 9:489–529
Fuentes-Landete V, Mitterdorfer C, Handle P, Ruiz G, Bernard J, Bogdan A, Seidl M, Amann-Winkel K, Stern J, Fuhrmann S et al (2015) Crystalline and amorphous ices. In: Proceedings of the International School of Physics "Enrico Fermi", vol 187, pp 173–208
Fukazawa H, Ikeda S, Mae S (1998) Incoherent inelastic neutron scattering measurements on ice XI; the proton-ordered phase of ice Ih doped with KoH. Chem Phys Lett 282:215–218
Gainaru C, Vynokur E, Köster K, Fuentes-Landete V, Spettel N, Zollner J, Loerting T, Böhmer R (2018) Dynamic signatures of the transition from stacking disordered to hexagonal ice: dielectric and nuclear magnetic resonance studies. J Chem Phys 148:134502
Gallo P, Amann-Winkel K, Angell CA, Anisimov MA, Caupin F, Chakravarty C, Lascaris E, Loerting T, Panagiotopoulos AZ, Russo J et al (2016) Water: a tale of two liquids. Chem Rev 116:7463–7500
Gavish M, Popovitz-Biro R, Lahav M, Leiserowitz L (1990) Ice nucleation by alcohols arranged in monolayers at the surface of water drops. Science 250:973–975
Gianetti MM, Haji-Akbari A, Longinotti MP, Debenedetti PG (2016) Computational investigation of structure, dynamics and nucleation kinetics of a family of modified stillinger–weber model fluids in bulk and freestanding thin films. Phys Chem Chem Phys 18(5):4102–4111
Goncharov AF, Goldman N, Fried LE, Crowhurst JC, Kuo I-FW, Mundy CJ, Zaug JM (2005) Dynamic ionization of water under extreme conditions. Phys Rev Lett 94(12):125508
Goncharov AF, Sanloup C, Goldman N, Crowhurst JC, Bastea S, Howard W, Fried LE, Guignot N, Mezouar M, Meng Y (2009) Dissociative melting of ice vii at high pressure. J Chem Phys 130:124514
Gfańasy L, Pusztai T, James PF (2002) Interfacial properties deduced from nucleation experiments: a Cahn–Hilliard analysis. J Chem Phys 117:6157
Green JL, Angell CA (1989) Phase relations and vitrification in saccharide-water solutions and the trehalose anomaly. J Phys Chem 93:2880–2882
Gross EK, Dreizler RM (2013) Density functional theory, vol 337. Springer Science & Business Media, Berlin
Guillot B (2002) A reappraisal of what we have learnt during three decades of computer simulations on water. J Mol Liq 101:219–260
Guloy AM, Ramlau R, Tang Z, Schnelle W, Baitinger M, Grin Y (2006) A guest-free germanium clathrate. Nature 443:320

Haji-Akbari A (2016) Rating antifreeze proteins: not a breeze. Proc Natl Acad Sci U S A 113:3714–3716
Haji-Akbari A (2018) Forward-flux sampling with jumpy order parameters. J Chem Phys 149 (7):072303
Haji-Akbari A, Debenedetti PG (2015) Direct calculation of ice homogeneous nucleation rate for a molecular model of water. Proc Natl Acad Sci U S A 112:10582
Haji-Akbari A, Debenedetti PG (2017a) Computational investigation of surface freezing in a molecular model of water. Proc Natl Acad Sci U S A 114:3316–3321
Haji-Akbari A, Debenedetti PG (2017b) Perspective: surface freezing in water: a nexus of experiments and simulations. J Chem Phys 147:060901
Haji-Akbari A, DeFever RS, Sarupria S, Debenedetti PG (2014) Suppression of sub-surface freezing in free-standing thin films of monoatomic water. Phys Chem Chem Phys 16:25916–25927
Hales TC (2006) Historical overview of the Kepler conjecture. Discret Comput Geom 36:5–20
Handa YP, Klug D, Whalley E (1986) Difference in energy between cubic and hexagonal ice. J Chem Phys 84:7009–7010
Hemley R, Jephcoat A, Mao H, Zha C, Finger L, Cox D (1987) Static compression of H_2O-ice to 128 GPa (1.28 Mbar). Nature 330(6150):737
Hemley R, Chen L, Mao H (1989) New transformations between crystalline and amorphous ice. Nature 338:638
Herbert RJ, Murray BJ, Dobbie SJ, Koop T (2015) Sensitivity of liquid clouds to homogenous freezing parameterizations. Geophys Res Lett 42:1599–1605
Hermann A, Ashcroft N, Hoffmann R (2012) High pressure ices. Proc Natl Acad Sci U S A 109:745–750
Hirsch K, Holzapfel W (1984) Symmetric hydrogen bonds in ice X. Phys Lett A 101:142–144
Hoose C, Möhler O (2012) Heterogeneous ice nucleation on atmospheric aerosols: a review of results from laboratory experiments. Atmos Chem Phys 12:9817–9854
Hoose C, Kristjánsson JE, Chen J-P, Hazra A (2010) A classical theory-based parameterization of heterogeneous ice nucleation by mineral dust, soot, and biological particles in a global climate model. J Atmos Sci 67:2483–2503
Iglev H, Schmeisser M, Simeonidis K, Thaller A, Laubereau A (2006) Ultrafast superheating and melting of bulk ice. Nature 439:183
Isachenko V, Isachenko E, Katkov II, Montag M, Dessole S, Nawroth F, van der Ven H (2004) Cryoprotectant-free cryopreservation of human spermatozoa by vitrification and freezing in vapor: effect on motility, dna integrity, and fertilization ability. Biol Reprod 71:1167–1173
Jackson CL, McKenna GB (1990) The melting behavior of organic materials confined in porous solids. J Chem Phys 93:9002–9011
Jayaraman A, Klement W Jr, Kennedy G (1963) Melting and polymorphism at high pressures in some group IV elements and III-V compounds with the diamond/zincblende structure. Phys Rev 130:540
Jensen EJ, Toon OB (1997) The potential impact of soot particles from aircraft exhaust on cirrus clouds. Geophys Res Lett 24:249–252
Johari G (1997) The Gibbs–Thomson effect and intergranular melting in ice emulsions: interpreting the anomalous heat capacity and volume of super cooled water. J Chem Phys 107:10154–10165
Johari G (1998) Liquid state of low-density pressure-amorphized ice above its T_g. J Phys Chem B 102:4711–4714
Johari G (2005) Water's size-dependent freezing to cubic ice. J Chem Phys 122:194504
Johari G, Hallbrucker A, Mayer E (1996) Two calorimetrically distinct states of liquid water below 150 kelvin. Science 273:90–92
Johnson CA (1965) Generalization of the Gibbs-Thomson equation. Surf Sci 3:429–444
Johnston JC, Molinero V (2012) Crystallization, melting, and structure of water nanoparticles at atmospherically relevant temperatures. J Am Chem Soc 134:6650–6659

Johnston JC, Kastelowitz N, Molinero V (2010) Liquid to quasicrystal transition in bilayer water. J Chem Phys 133:154516
Joly M, Attard E, Sancelme M, Deguillaume L, Guilbaud C, Morris CE, Amato P, Delort A-M (2013) Ice nucleation activity of bacteria isolated from cloud water. Atmos Environ 70:392–400
Jones D (1974) The free energies of solid-liquid interfaces. J Mater Sci 9:1–17
Jones EB, Stevanovíc V (2017) Polymorphism in elemental silicon: probabilistic interpretation of the realizability of metastable structures. Phys Rev B 96:184101
Kamb B (1964) Ice. II. A proton-ordered form of ice. Acta Crystallogr 17:1437–1449
Kamb B, Davis BL (1964) Ice VII, the densest form of ice. Proc Natl Acad Sci U S A 52:1433–1439
Kaneko T, Bai J, Yasuoka K, Mitsutake A, Zeng XC (2013) New computational approach to determine liquid–solid phase equilibria of water confined to slit nanopores. J Chem Theory Comput 9(8):3299–3310
Kanno H, Angell CA (1977) Homogeneous nucleation and glass formation in aqueous alkali halide solutions at high pressures. J Phys Chem 81:2639–2643
Kastelowitz N, Johnston JC, Molinero V (2010) The anomalously high melting temperature of bilayer ice. J Chem Phys 132(12):124511
Kauzmann W, Eisenberg D (1969) The structure and properties of water. Clarendon Press, Oxford
Kiselev A, Bachmann F, Pedevilla P, Cox SJ, Michaelides A, Gerthsen D, Leisner T (2017) Active sites in heterogeneous ice nucleation—the example of K-rich feldspars. Science 355:367–371
Klotz S, Strässle T, Saitta A, Rousse G, Hamel G, Nelmes R, Loveday J, Guthrie M (2005) In situ neutron diffraction studies of high density amorphous ice under pressure. J Phys Condens Matter 17:S967
Knight C, DeVries A (1989) Melting inhibition and superheating of ice by an antifreeze glycopeptide. Science 245:505–507
Knight CA, De Vries AL, Oolman LD (1984) Fish antifreeze protein and the freezing and recrystallization of ice. Nature 308:295
Knopf DA, Alpert PA (2013) A water activity based model of heterogeneous ice nucleation kinetics for freezing of water and aqueous solution droplets. Faraday Discuss 165:513–534
Knopf DA, Rigg YJ (2011) Homogeneous ice nucleation from aqueous inorganic/organic particles representative of biomass burning: water activity, freezing temperatures, nucleation rates. J Phys Chem A 115(5):762–773
Knopf DA, Alpert PA, Wang B, Aller JY (2011) Stimulation of ice nucleation by marine diatoms. Nat Geosci 4(2):88–90
Knott BC, Molinero V, Doherty MF, Peters B (2012) Homogeneous nucleation of methane hydrates: unrealistic under realistic conditions. J Am Chem Soc 134:19544–19547
Koga K, Zeng XC, Tanaka H (1997) Freezing of confined water: a bilayer ice phase in hydrophobic nanopores. Phys Rev Lett 79:5262
Koga K, Gao G, Tanaka H, Zeng XC (2001) Formation of ordered ice nanotubes inside carbon nanotubes. Nature 412:802
Kohl I, Mayer E, Hallbrucker A (2000) The glassy water–cubic ice system: a comparative study by X-ray diffraction and differential scanning calorimetry. Phys Chem Chem Phys 2:1579–1586
Kolafa J (2014) Residual entropy of ices and clathrates from Monte Carlo simulation. J Chem Phys 140:204507
König H (1943) Eine kubische eismodifikation. Z Kristallogr 105:279–286
Koop T (2004) Homogeneous ice nucleation in water and aqueous solutions. Z Phys Chem 218:1231–1258
Koop T, Luo B, Tsias A, Peter T (2000) Water activity as the determinant for homogeneous ice nucleation in aqueous solutions. Nature 406:611–614
Kristensen J, Cotterill R (1977) On the existence of pre-melting and after melting effects a neutron scattering investigation. Philos Mag 36:437–452
Kuhn T, Earle ME, Khalizov AF, Sloan JJ (2011) Size dependence of volume and surface nucleation rates for homogeneous freezing of supercooled water droplets. Atmos Chem Phys 11:2853–2861

Kumar P, Buldyrev SV, Starr FW, Giovambattista N, Stanley HE (2005) Thermodynamics, structure, and dynamics of water confined between hydrophobic plates. Phys Rev E 72:051503
Kuwayama M, Vajta G, Kato O, Leibo SP (2005) Highly efficient vitrification method for cryopreservation of human oocytes. Reprod BioMed Online 11(3):300–308
Laksmono H, McQueen TA, Sellberg JA, Loh ND, Huang C, Schlesinger D, Sierra RG, Hampton CY, Nordlund D, Beye M, Martin AV, Barty A, Seibert MM, Messerschmidt M, Williams GJ, Boutet S, Amann-Winkel K, Loerting T, Pettersson LGM, Bogan MJ, Nilsson A (2015) Anomalous behavior of the homogeneous ice nucleation rate in "no-man's land". J Phys Chem Lett 6:2826–2832
Lemke S, Handle PH, Plaga LJ, Stern JN, Seidl M, Fuentes-Landete V, Amann-Winkel K, Köster KW, Gainaru C, Loerting T et al (2017) Relaxation dynamics and transformation kinetics of deeply super cooled water: temperature, pressure, doping, and proton/deuteron isotope effects. J Chem Phys 147(3):034506
Li J, Chen H, Stone HA (2013a) Ice lubrication for moving heavy stones to the forbidden city in 15th- and 16th-century China. Proc Natl Acad Sci U S A 110:20023–20027
Li T, Donadio D, Galli G (2013b) Ice nucleation at the nanoscale probes no man's land of water. Nat Commun 4:1887
Lindemann F (1910) Fa lindemann. Phys Z 11:609
Loerting T, Salzmann C, Kohl I, Mayer E, Hallbrucker A (2001) A second distinct structural "state" of high-density amorphous ice at 77 k and 1 bar. Phys Chem Chem Phys 3:5355–5357
Lupi L, Hudait A, Peters B, Grünwald M, Mullen RG, Nguyen AH, Molinero V (2017) Role of stacking disorder in ice nucleation. Nature 551:218–222
Malkin TL, Murray BJ, Brukhno AV, Anwar J, Salzmann CG (2012) Structure of ice crystallized from supercooled water. Proc Natl Acad Sci U S A 109:1041–1045
Malkin TL, Murray BJ, Salzmann CG, Molinero V, Pickering SJ, Whale TF (2015) Stacking disorder in ice I. Phys Chem Chem Phys 17:60–76
Maslin M, Owen M, Betts R, Day S, Jones TD, Ridgwell A (2010) Gas hydrates: past and future geohazard? Philos Trans R Soc A 368:2369–2393
Mayer E (1985) New method for vitrifying water and other liquids by rapid cooling of their aerosols. J Appl Phys 58:663–667
Mayer E, Hallbrucker A (1987) Cubic ice from liquid water. Nature 325:601
Mayer E, Pletzer R (1986) Astrophysical implications of amorphous ice—a microporous solid. Nature 319:298
Mercury L, Vieillard P, Tardy Y (2001) Thermodynamics of ice polymorphs and 'ice-like' water in hydrates and hydroxides. Appl Geochem 16:161–181
Meryman HT (1956) Mechanics of freezing in living cells and tissues. Science 124:515–521
Millot M, Coppari F, Rygg JR, Barrios AC, Hamel S, Swift DC, Eggert JH (2019) Nanosecond X-ray diffraction of shock-compressed superionic water ice. Nature 569:251
Mishima O, Calvert LD, Whalley E (1984) Melting ice' I at 77 K and 10 kbar: a new method of making amorphous solids. Nature 310:393–395
Mishima O, Calvert L, Whalley E (1985) An apparently first-order transition between two amorphous phases of ice induced by pressure. Nature 314:76
Mitchell EH, Raut U, Teolis BD, Baragiola RA (2017) Porosity effects on crystallization kinetics of amorphous solid water: implications for cold icy objects in the outer solar system. Icarus 285:291–299
Mochizuki K, Matsumoto M, Ohmine I (2013) Defect pair separation as the controlling step in homogeneous ice melting. Nature 498:350
Molinero V, Moore EB (2009) Water modeled as an intermediate element between carbon and silicon. J Phys Chem B 113:4008–4016
Moore EB, Molinero V (2010) Ice crystallization in water's "no-man's land". J Chem Phys 132:244504
Moore EB, Molinero V (2011a) Is it cubic? Ice crystallization from deeply supercooled water. Phys Chem Chem Phys 13:20008–20016

Moore EB, Molinero V (2011b) Structural transformation in supercooled water controls the crystallization rate of ice. Nature 479:506–508
Moore EB, Allen JT, Molinero V (2012) Liquid-ice coexistence below the melting temperature for water confined in hydrophilic and hydrophobic nanopores. J Phys Chem C 116:7507–7514
Morishige K, Uematsu H (2005) The proper structure of cubic ice confined in mesopores. J Chem Phys 122:044711
Morishige K, Yasunaga H, Uematsu H (2009) Stability of cubic ice in mesopores. J Phys Chem C 113:3056–3061
Muldrew K, McGann LE (1990) Mechanisms of intracellular ice formation. Biophys J 57 (3):525–532
Muldrew K, McGann LE (1994) The osmotic rupture hypothesis of intracellular freezing injury. Biophys J 66:532–541
Mullen RG, Shea J-E, Peters B (2015) Easy transition path sampling methods: flexible-length aimless shooting and permutation shooting. J Chem Theory Comput 11:2421–2428
Murray BJ (2008) Enhanced formation of cubic ice in aqueous organic acid droplets. Environ Res Lett 3(2):025008
Murray BJ, Bertram AK (2007) Strong dependence of cubic ice formation on aqueous droplet ammonium to sulphate ratio. In: O'Dowd CD, Wagner PE (eds) Nucleation and atmospheric aerosols. Springer, Dordrecht, pp 432–435
Murray BJ, Knopf DA, Bertram AK (2005) The formation of cubic ice under conditions relevant to earth's atmosphere. Nature 434:202–205
Murray BJ, O'Sullivan D, Atkinson JD, Webb ME (2012) Ice nucleation by particles immersed in supercooled cloud droplets. Chem Soc Rev 41:6519–6554
O'Sullivan D, Murray BJ, Ross JF, Whale TF, Price HC, Atkinson JD, Umo NS, Webb ME (2015) The relevance of nanoscale biological fragments for ice nucleation in clouds. Sci Rep 5:8082
Olijve LLC, Meister K, Devries AL, Duman JG, Guo S, Bakker HJ, Voets IK (2016) Blocking rapid ice crystal growth through non-basal plane adsorption of antifreeze proteins. Proc Natl Acad Sci U S A 113:3740–3745
Oxtoby DW (1992) Homogeneous nucleation: theory and experiment. J Phys Condens Matter 4:7627
Padayachee K, Watt MP, Edwards N, Mycock DJ (2009) Cryopreservation as a tool for the conservation of Eucalyptus genetic variability: concepts and challenges. South Forests 71:165–170
Palmer JC, Martelli F, Liu Y, Car R, Panagiotopoulos AZ, Debenedetti PG (2014) Metastable liquid–liquid transition in a molecular model of water. Nature 510:385–388
Palmer JC, Haji-Akbari A, Singh RS, Martelli F, Car R, Panagiotopoulos AZ, Debenedetti PG (2018a) Comment on "The putative liquid-liquid transition is a liquid-solid transition in atomistic models of water" [I and II: J. Chem. Phys. 135, 134503 (2011); J. Chem. Phys. 138, 214504 (2013)]. J Chem Phys 148:137101
Palmer JC, Poole PH, Sciortino F, Debenedetti PG (2018b) Advances in computational studies of the liquid–liquid transition in water and water-like models. Chem Rev 118:9129–9151
Petrenko VF (1993) Structure of ordinary Ice Ih. Part 1: Ideal structure of ice. Technical report, Thayer School of Engineering, Hanover NH
Petrenko VF, Whitworth RW (1999) Physics of ice. Oxford University Press, Oxford
Pluhárová E, Vrbka L, Jungwirth P (2010) Effect of surface pollution on homogeneous ice nucleation: a molecular dynamics study. J Phys Chem C 114:7831–7838
Poole PH, Sciortino F, Essmann U, Stanley E (1992) Phase behaviour of metastable water. Nature 360:324–328
Popovitz-Biro R, Wang J, Majewski J, Shavit E, Leiserowitz L, Lahav L (1994) Induced freezing of supercooled water into ice by self-assembled crystalline monolayers of amphiphilic alcohols at the air-water interface. J Am Chem Soc 116:1179–1191
Potapczuk MG (2013) Aircraft icing research at NASA Glenn Research Center. J Aerosp Eng 26:260–276

Privalov PL (1990) Cold denaturation of protein. Crit Rev Biochem Mol 25:281–306
Rall W (1987) Factors affecting the survival of mouse embryos cryopreserved by vitrification. Cryobiology 24:387–402
Rall WF, Fahy GM (1985) Ice-free cryopreservation of mouse embryos at −196°c by vitrification. Nature 313(6003):573
Reinhardt A, Doye JPK (2012) Free energy landscapes for homogeneous nucleation of ice for a monatomic water model. J Chem Phys 136:054501
Reinhardt A, Doye JPK, Noya EG, Vega C (2012) Local order parameters for use in driving homogeneous ice nucleation with all-atom models of water. J Chem Phys 137:194504
Ronchi C, Hiernaut J (1996) Experimental measurement of pre-melting and melting of thorium dioxide. J Alloys Compd 240:179–185
Rosinski J (1980) Heterogeneous nucleation of ice on surfaces of liquids. J Phys Chem 84:1829–1832
Rosinski J, Lecinski A (1981) Further studies of heterogeneous nucleation of ice at the liquid-liquid interface. J Phys Chem 85:2993–2997
Rosinski J, Kopcewicz B, Sandoval N (1990) Heterogeneous nucleation of ice at the liquid-liquid interface. J Aerosol Sci 21(1):87–96
Rozmanov D, Kusalik PG (2012) Anisotropy in the crystal growth of hexagonal ice, I-h. J Chem Phys 137:094702
Russo J, Romano F, Tanaka H (2014) New metastable form of ice and its role in the homogeneous crystallization of water. Nat Mater 13:733–739
Saika-Voivod I, Sciortino F, Poole PH (2000) Computer simulations of liquid silica: equation of state and liquid–liquid phase transition. Phys Rev E 63(1):011202
Salzmann CG, Radaelli PG, Mayer E, Finney JL (2009) Ice XV: a new thermodynamically stable phase of ice. Phys Rev Lett 103:105701
Samanta A, Tuckerman ME, Yu T-Q, Weinan E (2014) Microscopic mechanisms of equilibrium melting of a solid. Science 346:729–732
Sánchez MA, Kling T, Ishiyama T, van Zadel M-J, Bisson PJ, Mezger M, Jochum MN, Cyran JD, Smit WJ, Bakker HJ et al (2017) Experimental and theoretical evidence for bilayer-by-bilayer surface melting of crystalline ice. Proc Natl Acad Sci U S A 114:227–232
Sanz E, Vega C, Espinosa JR, Caballero-Bernal R, Abascal JLF, Valeriani C (2013) Homogeneous ice nucleation at moderate supercooling from molecular simulation. J Am Chem Soc 135:15008–15017
Sastry S, Angell CA (2003) Liquid–liquid phase transition in supercooled silicon. Nat Mater 2:739
Sastry S, Debenedetti PG, Sciortino F, Stanley HE (1996) Singularity free interpretation of the thermodynamics of supercooled water. Phys Rev E 53:6144
Schumann U, Weinzierl B, Reitebuch O, Schlager H, Minikin A, Forster C, Baumann R, Sailer T, Graf K, Mannstein H, Voigt C, Rahm S, Simmet R, Scheibe M, Lichtenstern M, Stock P, Rüba H, Schäuble D, Tafferner A, Rautenhaus M, Gerz T, Ziereis H, Krautstrunk M, Mallaun C, Gayet J-F, Lieke K, Kandler K, Ebert M, Weinbruch S, Stohl A, Gasteiger J, Grob S, Freudenthaler V, Wiegner M, Ansmann A, Tesche M, Olafsson H, Sturm K (2011) Airborne observations of the Eyjafjalla Volcano ash cloud over Europe during air space closure in April and May 2010. Atmos Chem Phys 11:2245–2279
Schwager B, Chudinovskikh L, Gavriliuk A, Boehler R (2004) Melting curve of H_2O to 90 gpa measured in a laser-heated diamond cell. J Phys Condens Matter 16:S1177
Seeley L, Seidler G (2001) Two-dimensional nucleation of ice from super cooled water. Phys Rev Lett 87:055702
Seidl M, Amann-Winkel K, Handle PH, Zifferer G, Loerting T (2013) From parallel to single crystallization kinetics in high-density amorphous ice. Phys Rev B 88:174105
Sellberg JA, Huang C, McQueen TA, Loh ND, Laksmono H, Schlesinger D, Sierra RG, Nordlund D, Hampton CY, Starodub D, DePonte DP, Beye M, Chen C, Martin AV, Barty A, Wikfeldt KT, Weiss TM, Caronna C, Feldkamp J, Skinner LB, Seibert MM, Messerschmidt M,

Williams GJ, Boutet S, Pettersson LGM, Bogan MJ, Nilsson A (2014) Ultrafast X-ray probing of water structure below the homogeneous ice nucleation temperature. Nature 510:381–384
Seo M, Jang E, Kim K, Choi S, Kim JS (2012) Understanding anisotropic growth behavior of hexagonal ice on a molecular scale: a molecular dynamics simulation study. J Chem Phys 137:154503
Shilling J, Tolbert M, Toon O, Jensen E, Murray BJ, Bertram AK (2006) Measurements of the vapor pressure of cubic ice and their implications for atmospheric ice clouds. Geophys Res Lett 33:L17801
Shultz MJ, Brumberg A, Bisson PJ, Shultz R (2015) Producing desired ice faces. Proc Natl Acad Sci U S A 112:E6096–E6100
Sigurbjörnsson OF, Signorell R (2008) Volume versus surface nucleation in freezing aerosols. Phys Rev E 77:051601
Sliwinska-Bartkowiak M, Jazdzewska M, Huang L, Gubbins KE (2008) Melting behavior of water in cylindrical pores: carbon nanotubes and silica glasses. Phys Chem Chem Phys 10:4909–4919
Smallenburg F, Filion L, Sciortino F (2014) Erasing no-man's land by thermodynamically stabilizing the liquid–liquid transition in tetrahedral particles. Nat Phys 10:653
Song M, Yamawaki H, Fujihisa H, Sakashita M, Aoki K (2003) Infrared investigation on ice VIII and the phase diagram of dense ices. Phys Rev B 68:014106
Speedy RJ (1982) Limiting forms of the thermodynamic divergences at the conjectured stability limits in superheated and supercooled water. J Phys Chem 86:3002–3005
Stanley HE, Teixeira J (1980) Interpretation of the unusual behavior of H_2O and D_2O at low temperatures: tests of a percolation model. J Chem Phys 73:3404–3422
Stanley HE, Teixeira J, Geiger A, Blumberg R (1981) Interpretation of the unusual behavior of H_2O and D_2O at low temperature: are concepts of percolation relevant to the "puzzle of liquid water"? Physica A 106:260–277
Steytler D, Dore J, Wright C (1983) Neutron diffraction study of cubic ice nucleation in a porous silica network. J Phys Chem 87:2458–2459
Stokely K, Mazza MG, Stanley HE, Franzese G (2009) Effect of hydrogen bond cooperativity on the behavior of water. Proc Natl Acad Sci U S A 107:1301–1306
Strobel TA, Somayazulu M, Sinogeikin SV, Dera P, Hemley RJ (2016) Hydrogen-stuffed, quartz-like water ice. J Am Chem Soc 138:13786–13789
Swanson BD (2009) How well does water activity determine homogeneous ice nucleation temperature in aqueous sulfuric acid and ammonium sulfate droplets? J Atmos Sci 66:741–754
Tabazadeh A, Djikaev YS, Reiss H (2002) Surface crystallization of supercooled water in clouds. Proc Natl Acad Sci U S A 99:15873–15878
Takahashi T (1982) On the role of cubic structure in ice nucleation. J Cryst Growth 59:441–449
Takaiwa D, Hatano I, Koga K, Tanaka H (2008) Phase diagram of water in carbon nanotubes. Proc Natl Acad Sci U S A 105:39–43
ten Wolde PR, Frenkel D (1999) Homogeneous nucleation and the Ostwald step rule. Phys Chem Chem Phys 1:2191–2196
ten Wolde PR, Ruiz-Montero MJ, Frenkel D (1996) Numerical calculation of the rate of crystal nucleation in a Lennard-Jones system at moderate undercooling. J Chem Phys 104:9932–9947
Thomson W (1872) 4. On the equilibrium of vapour at a curved surface of liquid. Proc R Soc Edin 7:63–68
Turnbull D (1950) Kinetics of heterogeneous nucleation. J Chem Phys 18:198–203
Van Santen R (1984) The Ostwald step rule. J Phys Chem 88:5768–5769
Varshney D, Singh M (2015) History of lyophilization. In: Varshney D, Singh M (eds) Lyophilized biologics and vaccines. Springer, New York, pp 3–10
Vega C, Abascal JLF (2011) Simulating water with rigid non-polarizable models: a general perspective. Phys Chem Chem Phys 13:19663–19688
Volmer M, Flood H (1934) Tröpfchenbildung in dämpfen. Z Phys Chem 170:273–285
Voorhees PW (1985) The theory of Ostwald ripening. J Stat Phys 38:231–252

Vrbka L, Jungwirth P (2006) Homogeneous freezing of water starts in the subsurface. J Phys Chem B 110:18126–18129
Wang Z, Wang F, Peng Y, Zheng Z, Han Y (2012) Imaging the homogeneous nucleation during the melting of superheated colloidal crystals. Science 338:87–90
Wang Z, Wang F, Peng Y, Han Y (2015) Direct observation of liquid nucleus growth in homogeneous melting of colloidal crystals. Nat Commun 6:6942
Weertman J (1957) On the sliding of glaciers. J Glaciol 3(21):33–38
Wilson DR, Ballard SP (1999) A microphysically based precipitation scheme for the UK Meteorological Office unified model. Q J R Meteor Soc 125:1607–1636
Wilson PW, Haymet ADJ (2009) Effect of solutes on the heterogeneous nucleation temperature of supercooled water: an experimental determination. Phys Chem Chem Phys 11:2679–2682
Wilson TW, Ladino LA, Alpert PA, Breckels MN, Brooks IM, Browse J, Burrows SM, Carslaw KS, Huffman JA, Judd C, Kilthau WP, Mason RH, McFiggans G, Miller LA, Nájera JJ, Polishchuk E, Rae S, Schiller CL, Si M, Temprado JV, Whale TF, Wong JPS, Wurl O, Yakobi-Hancock JD, Abbatt JPD, Aller JY, Bertram AK, Knopf DA, Murray BJ (2015) A marine biogenic source of atmospheric ice-nucleating particles. Nature 525:234–238
Winkel K, Elsaesser MS, Mayer E, Loerting T (2008) Water polyamorphism: reversibility and (dis) continuity. J Chem Phys 128:044510
Xu L, Kumar P, Buldyrev SV, Chen S-H, Poole PH, Sciortino F, Stanley HE (2005) Relation between the widom line and the dynamic crossover in systems with a liquid–liquid phase transition. Proc Natl Acad Sci U S A 102:16558–16562
Xu Q, Sharp I, Yuan C, Yi D, Liao C, Glaeser AM, Minor A, Beeman J, Ridgway MC, Kluth P et al (2006) Large melting-point hysteresis of Ge nanocrystals embedded in SiO_2. Phys Rev Lett 97:155701
Yang WJ, Mochizuki S (2003) Low temperature and cryogenic applications in medicine and surgery. In: Kakac S, Smirnov H, Avelino MR (eds) Low temperature and cryogenic refrigeration, NATO Science Series II: Mathematics, physics and chemistry. Springer, Dordrecht, pp 295–308
Ye Z, Wu J, Ferradi NE, Shi X (2013) Anti-icing for key highway locations: fixed automated spray technology. Can J Civ Eng 40:11–18
Yen F, Chi Z (2015) Proton ordering dynamics of H_2O ice. Phys Chem Chem Phys 17 (19):12458–12461
Zangi R, Mark AE (2003) Monolayer ice. Phys Rev Lett 91:025502
Zeng Q, Li K, Fen-Chong T (2015) Heterogeneous nucleation of ice from supercooled NaCl solution confined in porous cement paste. J Cryst Growth 409:1–9
Zhang X, Sun P, Yan T, Huang Y, Ma Z, Zou B, Zheng W, Zhou J, Gong Y, Sun CQ (2015) Water's phase diagram: from the notion of thermodynamics to hydrogen-bond cooperativity. Prog Solid State Ch 43:71–81
Zhao W-H, Bai J, Yuan L-F, Yang J, Zeng XC (2014a) Ferroelectric hexagonal and rhombic monolayer ice phases. Chem Sci 5:1757–1764
Zhao W-H, Wang L, Bai J, Yuan L-F, Yang J, Zeng XC (2014b) Highly confined water: two-dimensional ice, amorphous ice, and clathrate hydrates. Acc Chem Res 47:2505–2513
Zheligovskaya EA, Malenkov GG (2006) Crystalline water ices. Russ Chem Rev 75:57
Zhu W, Zhao W-H, Wang L, Yin D, Jia M, Yang J, Zeng XC, Yuan L-F (2016) Two-dimensional interlocked pentagonal bilayer ice: how do water molecules form a hydrogen bonding network? Phys Chem Chem Phys 18:14216–14221
Zimmermann F, Weinbruch S, Schütz L, Hofmann H, Ebert M, Kandler K, Worringen A (2008) Ice nucleation properties of the most abundant mineral dust phases. J Geophys Res 113:D23204
Zobrist B, Marcolli C, Peter T, Koop T (2008) Heterogeneous ice nucleation in aqueous solutions: the role of water activity. J Phys Chem A 112:3965–3975